

Numerical Construction of Quasi-Periodic Solutions Beyond Symplectic Integrators

Mingwei Fu¹ and Bin Shi*^{2,3}

¹School of Mathematical Sciences, University of Chinese Academy of Sciences, Beijing 100049, China

²Center for Mathematics and Interdisciplinary Sciences, Fudan University, Shanghai 200433, China

³Shanghai Institute for Mathematics and Interdisciplinary Sciences, Shanghai 200433, China

February 19, 2026

Abstract

Symplectic integrators are the established standard for long-term simulations of nearly-integrable Hamiltonian systems due to their preservation of geometric structures. However, they suffer from an inherent limitation: secular phase-shift errors. While the qualitative “shape” of invariant tori is preserved, the numerical solution gradually drifts along the torus, leading to a phase-lag accumulation that degrades long-term positional accuracy. Inspired by the Craig-Wayne-Bourgain (CWB) scheme, originally developed as an analytical tool for infinite-dimensional systems, we introduce a numerical operator that incorporates frequency updates into a dimension-enlarged Newton iteration to compute quasi-periodic solutions. Unlike conventional time-stepping integrators, our alternating numerical procedure eliminates phase-lag accumulation by directly solving for instantaneous positions and phase angles. Theoretically, provided sufficient computational resources, the phase error can be reduced arbitrarily, remaining independent of the total integration time. Our algorithm translates the Nash-Moser iteration into a practical numerical framework, marking a significant departure from traditional Kolmogorov-Arnold-Moser (KAM) theory. While KAM provides rigorous existence proofs, its requirement for global Diophantine conditions and the total exclusion of resonant sets render it numerically inaccessible. By employing a “step-by-step” exclusion process and incrementally enlarging the dimension, our algorithm resolves irrationality conditions locally. This approach demonstrates that the “numerical irrationality problem” is not an intrinsic barrier to computation, offering a constructive, executable alternative to the non-executable nature of global KAM-based methods.

1 Introduction

The Hamiltonian formulation provides the modern geometric framework for classical mechanics, describing the state of a conservative system by canonical coordinates $\mathbf{x} = (x_1, \dots, x_n)$ and $\mathbf{y} =$

*Corresponding author: binshi@fudan.edu.cn

(y_1, \dots, y_n) defined in a $2n$ -dimensional phase space. The time evolution is governed by Hamilton's canonical equations

$$\dot{\mathbf{x}} = -\frac{\partial H}{\partial \mathbf{y}}, \quad (1.1a)$$

$$\dot{\mathbf{y}} = \frac{\partial H}{\partial \mathbf{x}}, \quad (1.1b)$$

where the Hamiltonian function $H = H(\mathbf{x}; \mathbf{y}) = H(x_1, \dots, x_n; y_1, \dots, y_n)$ typically represents the total energy of the system and acts as the generator of the dynamics. Beyond a reformulation of Newton's laws, the Hamiltonian framework is inherently geometric. The phase space is naturally endowed with a canonical symplectic structure $\omega = d\mathbf{x} \wedge d\mathbf{y} = \sum_{j=1}^n dx_j \wedge dy_j$ and the resulting flow $\varphi_t : (\mathbf{x}(0), \mathbf{y}(0)) \mapsto (\mathbf{x}(t), \mathbf{y}(t))$ is a symplectomorphism that preserves the symplectic two-form exactly for all times [Arnol'd, 2013]. This geometric structure underpins the characteristic long-time behavior of conservative systems, including phase-space volume preservation and the existence of invariant tori in integrable systems.

For long-time numerical simulations, it is therefore of fundamental importance to preserve this symplectic structure under time discretization. Symplectic integrators are numerical schemes specifically designed for this purpose: their one-step update maps are symplectic transformations of phase space, ensuring that the discrete flow inherits the essential geometric structure of the continuous Hamiltonian system. The formal development of symplectic integrators began with Feng [1986], who provided the first rigorous proof that such schemes can be systematically constructed as symplectic maps. From an algorithmic viewpoint, early developments in structure-preserving discretizations can be traced back to De Vogelaere [1956], with practical higher-order methods later introduced by Ruth [1983] and Feng [1985]. By construction, symplectic integrators exhibit remarkable long-time stability and qualitative accuracy, most notably the absence of secular energy drift and the faithful reproduction of phase-space topology. The theoretical foundation is further clarified by backward error analysis, which interprets the numerical solution as the exact flow of a nearby modified Hamiltonian system. The systematic study of backward error analysis for structure-preserving methods was initiated by Feng [1991]. Sharp characterizations of truncation errors were subsequently developed by Yoshida [1993], while long-time backward error analysis and lifespan estimates were established by Hairer and Lubich [1997]; see also the comprehensive review by Hairer et al. [2003]. More recently, Jordan [2018] advocated symplectic integrators as a geometric framework for analyzing gradient-based optimization algorithms.

This geometric philosophy extends naturally to other structure-preserving problems. For general divergence-free vector fields, such as those arising in incompressible fluid dynamics, the corresponding goal is to construct volume-preserving integrators. Building upon insights from the classical ABC flow, Feng and Shang [1995] established a general framework for constructing such schemes, accompanied by rigorous proofs of convergence and structure-preservation. Moreover, Hairer and Lubich [2000] introduced a class of highly oscillatory systems motivated by variants of the Fermi-Pasta-Ulam (FPU) model, and investigated their long-time numerical energy behavior. Although such modified systems do not coincide exactly with the original physical models, they capture essential stiffness and multiscale features relevant to numerical analysis. The stiffness properties of ordinary differential equations were analyzed in detail by Hairer and Wanner [1996]. Furthermore, Cohen et al. [2003] introduced the framework of modulated Fourier expansions, demonstrating that the harmonic energy associated with the highly oscillatory components is nearly conserved over time intervals that are exponentially long with respect to the dominant frequency.

A class of systems of paramount importance is that of nearly integrable Hamiltonian systems. In action-angle variables $(\mathbf{I}, \boldsymbol{\theta}) = (I_1, \dots, I_n; \theta_1, \dots, \theta_n) \in \mathbb{R}_+^n \times \mathbb{T}^n$, the Hamiltonian takes the form

$$H = H(\mathbf{I}; \boldsymbol{\theta}) = H_0(\mathbf{I}) + \varepsilon H_1(\mathbf{I}, \boldsymbol{\theta}), \quad 0 < \varepsilon \ll 1, \quad (1.2)$$

where $I_j = (x_j^2 + y_j^2)/2$ and $\theta_j = \arctan(y_j/x_j)$. The unperturbed Hamiltonian $H_0(\mathbf{I})$ describes an integrable system with frequencies $\boldsymbol{\omega}(\mathbf{I}) := \nabla_{\mathbf{I}} H_0(\mathbf{I})$. One of the most profound achievements in twentieth-century dynamical systems theory is the Kolmogorov-Arnold-Moser (KAM) theorem [Arnold, 1963, Moser, 1962], which asserts that, under suitable nondegeneracy and smoothness conditions, a large measure of invariant tori for the unperturbed system persists under small Hamiltonian perturbations, albeit slightly deformed. These surviving KAM tori confine the motion and provide a profound mechanism for long-time stability, thereby explaining the absence of global chaos in weakly perturbed Hamiltonian systems. From a numerical perspective, the persistence of KAM tori can also be observed for symplectic integrators. Under appropriate step-size conditions, Shang [1999, 2000] established rigorous KAM-type theorems for symplectic discretizations. Nevertheless, as emphasized by Gauckler et al. [2018], the design of numerical algorithms with favorable long-time dynamical properties remains a central challenge.

1.1 Intrinsic limitation of symplectic integrators: secular drift of angle variables

We here consider the simple one-dimensional harmonic oscillator: $\ddot{x} = -x$. Introducing the auxiliary variable $y = -\dot{x}$, the system can be written in Hamiltonian form as

$$\begin{cases} \dot{x} = -y, \\ \dot{y} = x. \end{cases} \quad (1.3a)$$

$$(1.3b)$$

Equivalently, the dynamics are generated by the Hamiltonian $H = (x^2 + y^2)/2$, equipped with the canonical symplectic two-form $\omega = dx \wedge dy$. The contours of the Hamiltonian are circles in phase space, corresponding to periodic orbits with constant energy. Starting from the initial condition $x(0) = 1$ and $y(0) = \dot{x}(0) = 0$, the exact solution traces a circular trajectory in the (x, y) -plane, rotating counterclockwise with constant angular frequency $\omega = 1$. Equivalently, the phase angle evolves as $\theta(t) = t$; see Figure 1. Given a step size $h > 0$, we apply the simple first-order symplectic (forward-backward) integrator to the Hamilton system (1.3):

$$\begin{cases} x_{n+1} - x_n = -hy_n, \\ y_{n+1} - y_n = hx_{n+1}, \end{cases} \quad (1.4a)$$

$$(1.4b)$$

which can be written in matrix form as

$$\begin{pmatrix} x_{n+1} \\ y_{n+1} \end{pmatrix} = \begin{pmatrix} 1 & -h \\ h & 1 - h^2 \end{pmatrix} \begin{pmatrix} x_n \\ y_n \end{pmatrix} \triangleq M_h \begin{pmatrix} x_n \\ y_n \end{pmatrix}.$$

The eigenvalues of the symplectic map M_h are given by

$$\lambda_{\pm} = 1 - \frac{h^2}{2} \pm ih\sqrt{1 - \frac{h^2}{4}}. \quad (1.5)$$

For any $h \in [0, 2)$, these eigenvalues form a complex conjugate pair with unit modulus, $|\lambda_{\pm}| = 1$, implying that M_h is area-preserving; see Figure 1.

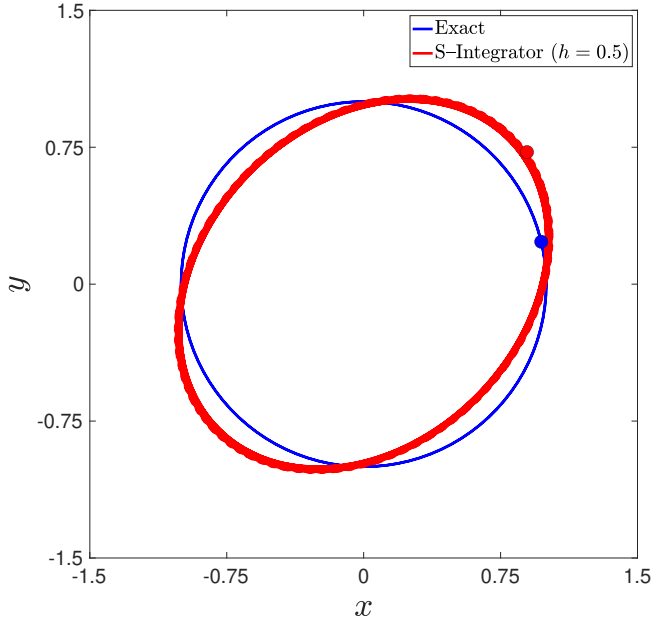


Figure 1: Phase space trajectories for both the exact solution of the Hamiltonian system (1.3) and the first-order symplectic integrator (1.4), starting from the initial $(x(0), y(0)) = (1, 0)$; markers indicate the states at $t_n = nh$ with $n = 101$.

As illustrated in Figure 1, although both the exact solution and the symplectic integrator generate closed circular orbits that remain close in phase space, their positions along the orbits, equivalently, their phase angles, do not coincide. To quantify the phase mismatch, we compute the numerical rotation angle per step, denoted by θ_h . Since the eigenvalues of M_h have unit modulus, there exists an invertible matrix S_h such that

$$M_h = S_h^{-1} \begin{pmatrix} \cos \theta_h & -\sin \theta_h \\ \sin \theta_h & \cos \theta_h \end{pmatrix} S_h. \quad (1.6)$$

Combining (1.5) and (1.6), it is straightforward to verify that

$$\cos \theta_h = 1 - \frac{h^2}{2}, \quad \sin \theta_h = h \sqrt{1 - \frac{h^2}{4}}. \quad (1.7)$$

Since the exact solution advances the phase by h per time step, we define the numerical phase error as $\Delta \theta_h := \theta_h - h$. For any $h \in [0, 2)$, a direct estimate from (1.7) yields:

$$\Delta \theta_h = \theta_h - h = \arccos \left(1 - \frac{h^2}{2} \right) - h \geq \frac{1}{24} h^3.$$

Consequently, after n time steps, the accumulated phase error satisfies

$$n \Delta \theta_h \geq \frac{1}{24} n h^3 = \frac{1}{24} t_n h^2,$$

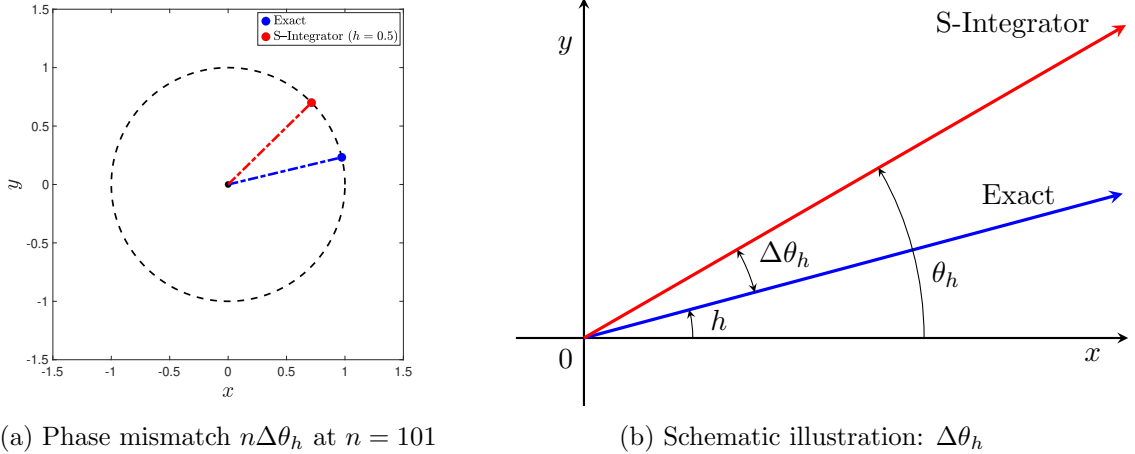


Figure 2: Accumulated phase (angle) error $n\Delta\theta_h$ at time $t_n = nh$ between the exact solution of the Hamiltonian system (1.3) and the first-order symplectic integrator (1.4).

where $t_n = nh$ denotes the physical time. This results in a secular drift in the numerical phase, as illustrated in Figure 2.

Figure 1 and Figure 2 demonstrate that, although symplectic integrators preserve the global geometric and topological structure of phase space, they do not, in general, guarantee uniform accuracy of the angle variables. Over long times, small local phase errors accumulate linearly in time, leading to an inevitable drift in the phase. In the long-time regime, while the numerical and exact trajectories remain close in shape, the precise position along the orbit becomes increasingly unpredictable, reflecting an intrinsic loss of phase fidelity.

2 A dimension-enlarged Newton scheme

The Craig-Wayne-Bourgain (CWB) scheme, originally developed by [Craig and Wayne \[1993\]](#), [Bourgain \[1994, 1998\]](#), is a fundamentally analytical framework for establishing the existence of quasi-periodic solutions. While extraordinarily powerful from a theoretical perspective, it has so far remained largely confined to existence proofs, and its potential as a practical numerical method has not been fully realized. At the core of the CWB approach lies a dimension-enlarged Newton (or Nash-Moser) iteration, which naturally suggests a viable computational strategy. In this work, we bridge this gap by transforming the analytic CWB framework into a concrete and implementable numerical algorithm. The proposed dimension-enlarged Newton scheme computes quasi-periodic solutions while preserving the underlying geometric structure of the system. Crucially, it avoids the secular phase-error drift inherent in standard symplectic integrators. In addition, the method is equipped with a rigorous a priori error bound, providing a quantitative certificate of accuracy and ensuring the reliability of the computed solutions.

2.1 Lattice representation

To begin our analysis, we introduce multi-index notation. for any $\alpha = (\alpha_1, \dots, \alpha_n) \in \mathbb{N}^n$ and $\mathbf{z} = (z_1, \dots, z_n) \in \mathbb{C}^n$, we define the length $|\alpha| := \sum_{i=1}^n |\alpha_i|$ and the associated monomial $\mathbf{z}^\alpha :=$

$\prod_{j=1}^n z_j^{\alpha_j}$. Consider the nearly integrable Hamiltonian system (1.2) in action-angle variables $(\mathbf{I}, \boldsymbol{\theta})$. We apply the complex canonical transformation $z_j = \sqrt{I_j} e^{i\theta_j}$ (and its conjugate $\bar{z}_j = \sqrt{I_j} e^{-i\theta_j}$), under which the symplectic form becomes $d\mathbf{z} \wedge d\bar{\mathbf{z}} = -id\mathbf{I} \wedge d\boldsymbol{\theta}$. In these coordinates, the Hamiltonian (1.2) is expressed as:

$$H(\mathbf{z}, \bar{\mathbf{z}}) = H_0(|z_1|^2, \dots, |z_n|^2) + \varepsilon H_1(\mathbf{z}, \bar{\mathbf{z}}), \quad (2.1)$$

where the unperturbed part H_0 depends only on the actions $I_j = |z_j|^2$, and the perturbation H_1 is a real-valued polynomial given by

$$H_1(\mathbf{z}, \bar{\mathbf{z}}) = \sum_{\boldsymbol{\alpha}, \boldsymbol{\beta}} h_{\boldsymbol{\alpha}\boldsymbol{\beta}} (z^{\boldsymbol{\alpha}} \bar{z}^{\boldsymbol{\beta}} + z^{\boldsymbol{\beta}} \bar{z}^{\boldsymbol{\alpha}}), \quad (2.2)$$

where the coefficients $h_{\boldsymbol{\alpha}\boldsymbol{\beta}}$ are real, and the total degree satisfies $\max\{|\boldsymbol{\alpha}| + |\boldsymbol{\beta}|\} \geq 3$. The resulting Hamiltonian equations of motion are

$$\dot{\mathbf{z}} = i\boldsymbol{\omega} \odot \mathbf{z} + i\varepsilon \frac{\partial H_1}{\partial \bar{\mathbf{z}}}, \quad (2.3)$$

where \odot denotes componentwise multiplication. Before proceeding, we recall the definition of a time-quasi-periodic function to set the stage for excluding resonant interactions.

Definition 2.1 (Quasi-Periodic Function). The frequency $\boldsymbol{\omega} \in \mathbb{R}^n$ is said to be *rationally independent* if it satisfies the non-resonance condition $\langle \mathbf{k}, \boldsymbol{\omega} \rangle \neq 0$ for any $\mathbf{k} \in \mathbb{Z}^n \setminus \{0\}$. A function $f = f(t)$ is called *time quasi-periodic* if there exists a periodic function $g = g(\boldsymbol{\theta})$ on the n -dimensional torus \mathbb{T}^n such that $f(t) = g(\boldsymbol{\omega}t)$.

For a vector-valued quasi-periodic function $\mathbf{z}(\boldsymbol{\omega}t) = (z_1(\boldsymbol{\omega}t), \dots, z_n(\boldsymbol{\omega}t))^\top$, we consider its Fourier decomposition:

$$\mathbf{z}(\boldsymbol{\omega}t) = \sum_{\mathbf{k} \in \mathbb{Z}^n} \hat{\mathbf{z}}(\mathbf{k}) e^{i\langle \mathbf{k}, \boldsymbol{\omega} \rangle t}, \quad (2.4)$$

where the coefficients $\{\hat{\mathbf{z}}(\mathbf{k})\}_{\mathbf{k} \in \mathbb{Z}^n}$ are indexed by the integer lattice \mathbb{Z}^n . In the unperturbed case ($\varepsilon = 0$), the system (2.3) is linear and completely integrable, admitting the explicit solution

$$z_j(\boldsymbol{\omega}t) = a_j e^{i\omega_j t}, \quad j = 1, \dots, n, \quad (2.5)$$

Given that the symplectic structure is invariant under the scaling $z_j \mapsto e a_j z_j$, we may assume without loss of generality that the amplitudes $a_j = e^{-1}$ for $j = 1, \dots, n$. The linear solution (2.5) corresponds to the Fourier representation (2.4) with coefficients localized on the standard basis vectors $\mathbf{e}_j \in \mathbb{Z}^n$ for $j = 1, \dots, n$:

$$\hat{z}_j(\mathbf{k}) = \begin{cases} a_j, & \mathbf{k} = \mathbf{e}_j, \\ 0, & \mathbf{k} \neq \mathbf{e}_j. \end{cases} \quad (2.6)$$

The solution to the nearly integrable Hamilton system (2.3) is treated as a perturbation of the linear solution (2.6), which admits the Fourier representation:

$$\mathbf{z}(\boldsymbol{\omega}'t) = \sum_{\mathbf{k} \in \mathbb{Z}^n} \hat{\mathbf{z}}(\mathbf{k}) e^{i\langle \mathbf{k}, \boldsymbol{\omega}' \rangle t}. \quad (2.7)$$

where $\boldsymbol{\omega}'$ represents a drifted frequency. This perturbed solution is characterized by the following properties:

- **Frequency drift:** The drifted frequency ω' remains close to the original frequency ω .
- **Fixed dominant modes:** The dominant Fourier coefficients remain fixed, with $\hat{z}_j(\mathbf{e}_j) = a_j$ for $j = 1, \dots, n$.
- **Perturbation-induced coefficients:** All remaining coefficients $\hat{z}_j(\mathbf{k}) \neq 0$ for $\mathbf{k} \neq \mathbf{e}_j$ are generated by the perturbation.

These resulting “excited” Fourier modes are expected to exhibit suitable decay properties, which will be established in the subsequent analysis. Our goal is to compute, numerically, a time quasi-periodic solution (2.7) to the perturbed system, starting from the linear solution (2.5). The overall numerical procedure, mapping the initial Fourier coefficients and frequency to their perturbed counterparts, is illustrated schematically in Figure 3.

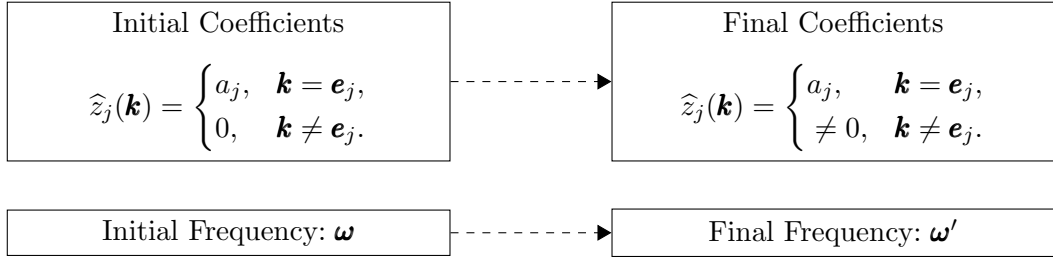


Figure 3: Schematic diagram of the numerical procedure.

2.2 Lyapunov-Schmidt decomposition

To facilitate the analysis, we denote the perturbation vector field by $\mathbf{X} = \partial H_1 / \partial \bar{\mathbf{z}}$, with its Fourier representation written as $\hat{\mathbf{X}} = \{\hat{\mathbf{X}}(\mathbf{k})\}_{\mathbf{k} \in \mathbb{Z}^n}$. Substituting the formal time quasi-periodic solution (2.7) into the complex Hamilton system (2.3), we derive the following algebraic system over the lattice \mathbb{Z}^n :

$$-\langle \mathbf{k}, \omega' \rangle \hat{\mathbf{z}} + \omega \odot \hat{\mathbf{z}} + \varepsilon \hat{\mathbf{X}}(\hat{\mathbf{z}}, \hat{\mathbf{z}}) = 0. \quad (2.8)$$

where the Fourier coefficients satisfy the symmetry condition $\hat{\mathbf{z}}(\mathbf{k}) = \overline{\hat{\mathbf{z}}(-\mathbf{k})}$. A key feature of the Fourier representation in (2.8) is that the initial state (2.6) is real. Given that the perturbation Hamiltonian H_1 is a multivariate polynomial with real coefficients, both the full vector field and its associated tangent linear operator are inherently real. The Newton scheme described in Section 2.3 preserves this reality, ensuring that all subsequent iterates remain real. Consequently, we may assume without loss of generality that the Fourier vector $\hat{\mathbf{z}}$ is real. Under this realness assumption, the symmetry condition simplifies to $\hat{\mathbf{z}}(\mathbf{k}) = \hat{\mathbf{z}}(-\mathbf{k})$, which implies that the perturbation vector field $\hat{\mathbf{X}}$ depends only on $\hat{\mathbf{z}}$, rather than depending on $\hat{\mathbf{z}}$ and $\hat{\mathbf{z}}$ independently. Therefore, the algebraic system (2.8) can be rewritten as:

$$-\langle \mathbf{k}, \omega' \rangle \hat{\mathbf{z}} + \omega \odot \hat{\mathbf{z}} + \varepsilon \hat{\mathbf{X}}(\hat{\mathbf{z}}) = 0. \quad (2.9)$$

Notice that when the perturbed frequency vector ω' coincides with the unperturbed vector ω , then the coefficient of $\hat{z}_j(\mathbf{k})$ in (2.9) vanishes for the mode $\mathbf{k} = \mathbf{e}_j$. This degeneracy motivates the

definition of the resonant set:

$$\mathcal{S} = \{(j, \mathbf{e}_j) \mid j = 1, \dots, n\}. \quad (2.10)$$

To handle the resulting singularities, we employ the Lyapunov-Schmidt decomposition, partitioning the algebraic system (2.9) into two subsystems according to whether the index pair (j, \mathbf{k}) belongs to the resonant set \mathcal{S} or not.

- **Q -equations (Resonant Modes):** For the resonant indices $(j, \mathbf{k}) \in \mathcal{S}$, specifically for $j = 1, \dots, n$ and $\mathbf{k} = \mathbf{e}_j$, the algebraic system (2.9) reduces to

$$(-\omega'_j + \omega_j) a_j + \varepsilon \hat{X}_j(\mathbf{e}_j) = 0, \quad (2.11)$$

which are referred to as the *Q -equations*. For convenience, we collect the resonant Fourier coefficients into the *resonant vector* $\hat{\mathbf{z}}_q := \mathbf{a} = (a_1, \dots, a_n)^\top$, and define the *resonant vector field* $\hat{\mathbf{X}}_q := (\hat{X}_1(\mathbf{e}_1), \dots, \hat{X}_n(\mathbf{e}_n))^\top$. Consequently, the Q -equations (2.11) can be written in the compact vector form as

$$(-\omega' + \omega) \odot \hat{\mathbf{z}}_q + \hat{\mathbf{X}}_q = 0. \quad (2.12)$$

- **P -equations (Non-Resonant Modes):** For non-resonant indices $(j, \mathbf{k}) \notin \mathcal{S}$, the corresponding components are collected into *non-resonant vector* $\hat{\mathbf{z}}_p$ and *non-resonant vector field* $\hat{\mathbf{X}}_p$. Accordingly, the full Fourier vector and vector field admit the following decomposition:

$$\hat{\mathbf{z}} = \begin{pmatrix} \hat{\mathbf{z}}_q \\ \hat{\mathbf{z}}_p \end{pmatrix} \quad \text{and} \quad \hat{\mathbf{X}} = \begin{pmatrix} \hat{\mathbf{X}}_q \\ \hat{\mathbf{X}}_p \end{pmatrix}. \quad (2.13)$$

By substituting the resonant components $\hat{\mathbf{z}}_p$ and $\hat{\mathbf{X}}_p$ into the algebraic system (2.9), we derive the *P -equations* as:

$$-\langle \mathbf{k}, \omega' \rangle \hat{\mathbf{z}}_p + \omega \odot \hat{\mathbf{z}}_p + \varepsilon \hat{\mathbf{X}}_p = 0. \quad (2.14)$$

To implement the Newton scheme for numerically computing the solution, we derive the tangent linear operator associated with the P -equations (2.14):

$$T = D + \varepsilon S, \quad (2.15)$$

where D denotes the diagonal operator with entries as $D_{j,\mathbf{k}} = -\langle \mathbf{k}, \omega' \rangle + \omega_j$ and $S = \partial \hat{\mathbf{X}}_p / \partial \hat{\mathbf{z}}_p$ arises from the nonlinear perturbation. The properties of S is discussed in Section 3.1.

2.3 Numerical scheme

Following the derivation of the P -equations (2.14), the central computational challenge lies in the treatment of the infinite-dimensional vector $\hat{\mathbf{z}}_p$. Traditional Newton methods typically require truncating the system to a fixed finite dimension. Once the problem is restricted to a finite lattice, however, truncation errors are inevitably introduced. In strongly nonlinear regimes, such errors do not vanish; instead, they may persist and accumulate, potentially growing as the iteration proceeds. To maintain computational tractability while ensuring that the truncation error converges

rigorously to zero, we employ a dimension-enlarged Newton scheme. This strategy draws inspiration from the Nash-Moser iteration, originally developed to overcome “small-divisor” difficulties in nonlinear analysis and to establish convergence within infinite-dimensional function spaces [Nash, 1956, Moser, 1966a,b].

To formalize the numerical procedure, we first define the truncated Fourier lattice box Λ_N for any positive integer $N \in \mathbb{N}$:

$$\Lambda_N := \left\{ \mathbf{k} \in \mathbb{Z}^n : \max_{1 \leq i \leq n} |\mathbf{k}_i| \leq N \right\}. \quad (2.16)$$

We then introduce the projection operator P_N , which restricts functions on the full lattice \mathbb{Z}^n to the truncated lattice Λ_N box:

$$(P_N \hat{\mathbf{z}})(\mathbf{k}) := \begin{cases} \hat{\mathbf{z}}(\mathbf{k}), & \text{if } \mathbf{k} \in \Lambda_N, \\ 0, & \text{if } \mathbf{k} \notin \Lambda_N. \end{cases} \quad (2.17)$$

For the tangent linear operator T , we define its restriction to the truncated lattice Λ_N as:

$$T_N := T|_{\mathbf{k} \in \Lambda_N} \quad (2.18)$$

Equivalently, consistent with the projection operator defined in (2.17), this restriction can be written as $T_N = P_N T P_N$.

With these preparation, we describe our alternating numerical scheme for updating the frequency and the non-resonant vector. Starting from the initial frequency $\omega^{(0)} = \omega$ and the initial non-resonant vector $\hat{\mathbf{z}}_p^{(0)} = \mathbf{0}$, we proceed iteratively. At the r -th step, the current approximations $\omega^{(r)}$ and $\hat{\mathbf{z}}_p^{(r)}$ serve as inputs for a two-stage process. First, we update the frequency by solving the Q -equations (2.12):

$$(-\omega^{(r+1)} + \omega) \odot \mathbf{a} + \varepsilon \hat{\mathbf{X}}_q(\hat{\mathbf{z}}_p^{(r)}; \mathbf{a}) = 0 \quad (2.19)$$

Next, we update the non-resonant vector via the P -equations (2.14). To this end, we define the full non-resonant vector field:

$$F(\omega, \hat{\mathbf{z}}_p; \mathbf{a}) = -\langle \mathbf{k}, \omega' \rangle \hat{\mathbf{z}}_p + \omega \odot \hat{\mathbf{z}}_p + \varepsilon \hat{\mathbf{X}}_p(\hat{\mathbf{z}}_p; \mathbf{a}). \quad (2.20)$$

Departing from classical existence theories for quasi-periodic solutions (see Bourgain [1994, 1998]), numerically efficiency necessitates an additional rank-one operator. This operator is derived from the Q -equations (2.12) to stabilize the frequency iteration:

$$B = -\frac{1}{e} \left(\frac{\partial \langle \mathbf{k}, \hat{\mathbf{X}}_q \rangle}{\partial \hat{\mathbf{z}}_p} \right) \hat{\mathbf{z}}_p^\top \quad (2.21)$$

Let $M \in \mathbb{N}$ be a fixed positive integer. We set the truncation dimension at the r -th step as $N_{r+1} := M^{r+1}$, so that the dimension of the truncated space increases by a factor of M at each iteration. The updated non-resonant vector is then obtained via a dimension-enlarged Newton step:

$$\hat{\mathbf{z}}_p^{(r+1)} = \hat{\mathbf{z}}_p^{(r)} - \left[(T + \varepsilon B)_{N_{r+1}}^{-1}(\hat{\mathbf{z}}_p^{(r)}, \omega^{(r+1)}; \mathbf{a}) \right] F(\hat{\mathbf{z}}_p^{(r)}, \omega^{(r+1)}; \mathbf{a}), \quad (2.22)$$

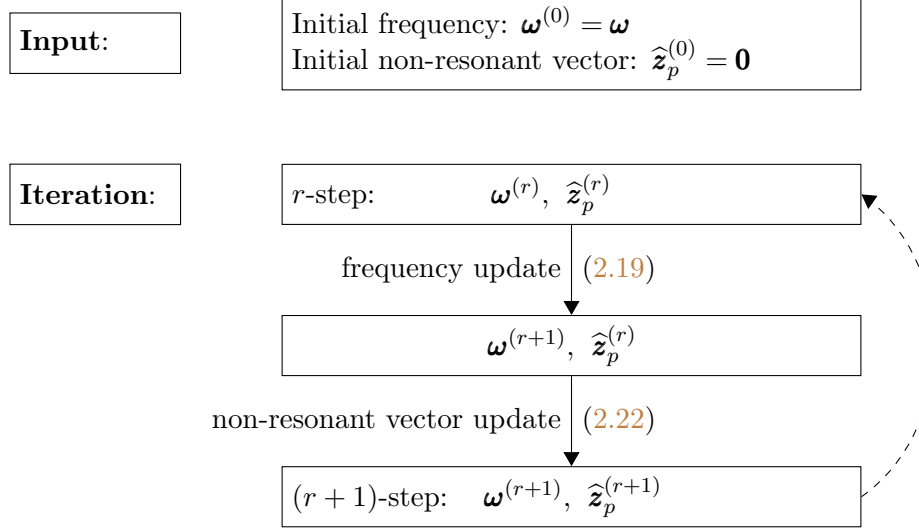


Figure 4: A diagram illustrating the alternating numerical procedure.

where the non-resonant vector $\hat{z}_p^{(r)}$ is supported on the lattice box Λ_{N_r} , while the updated vector $\hat{z}_p^{(r+1)}$ resides in the enlarged lattice box $\Lambda_{N_{r+1}}$. The alternating numerical procedure is illustrated in Figure 4.

This progressive enlargement is a hallmark of the Nash-Moser strategy: higher-frequency modes are gradually activated as the truncation dimension increases. This allows the scheme to approximate the infinite-dimensional solution while maintaining control over the inverse of the linearized operator. Although the norm of the inverse may grow as the dimension increases, the super-exponential convergence of the Newton update compensates for this growth, thereby ensuring that the scheme converges toward the true solution.

2.4 Statement of the main theorem

To establish the convergence theorem, we first define the norms necessary to quantify the infinite-dimensional vectors. For any Fourier vector $\hat{\mathbf{z}} = \{\hat{\mathbf{z}}(\mathbf{k})\}_{\mathbf{k} \in \mathbb{Z}^n}$, the ℓ_2 -norm is given by

$$\|\hat{\mathbf{z}}\|_2 = \left(\sum_{\mathbf{k} \in \mathbb{Z}^n} \|\hat{\mathbf{z}}(\mathbf{k})\|_2^2 \right)^{\frac{1}{2}}$$

Given that the continuous differentiability of the solution with respect to parameter, we know that the Fourier vector $\hat{\mathbf{z}}$ is a function of the frequency. Accordingly, we define the normed space $\mathcal{H}(\mathbb{Z}^n)$ as follows:

$$\mathcal{H}(\mathbb{Z}^n) = \left\{ \hat{\mathbf{z}} = \{\hat{\mathbf{z}}(\mathbf{k})\}_{\mathbf{k} \in \mathbb{Z}^n} \mid \hat{\mathbf{z}}(\mathbf{k}) \in \mathbb{R}^n, \|\hat{\mathbf{z}}\| = \|\hat{\mathbf{z}}\|_2 + \|\partial_{\omega} \hat{\mathbf{z}}\|_2 < \infty \right\}. \quad (2.23)$$

where the composite norm is given by $\|\cdot\| = \|\cdot\|_2 + \|\partial_{\omega}(\cdot)\|_2$. Unless otherwise specified, the composite norm $\|\cdot\|$ is used throughout this paper. In addition, $|\cdot|$ and $|\cdot|_{\infty}$ denote ℓ^1 -norm and ℓ^{∞} -norm, respectively, in \mathbb{Z}^n or \mathbb{R}^n . To characterize the regularity of the solutions, we define

Gevrey decay set within the ℓ_2 space as:

$$\mathcal{K}(s) = \left\{ \widehat{\mathbf{z}} \in \mathcal{H}(\mathbb{Z}^n) \mid \sup_{\mathbf{k} \in \mathbb{Z}^n} (\|\widehat{\mathbf{z}}(\mathbf{k})\| \exp\{|\mathbf{k}|^s\}) \leq 1 \right\}, \quad (2.24)$$

where the sub-exponential decay of the Fourier coefficients is essential for maintaining the regularity of the iterative scheme.¹ We now present the main theoretical statement of this study: the a priori error estimate for the alternating numerical procedure illustrated in Figure 4.

Theorem 2.2 (Convergence and Error Estimation). Let $\Omega \subseteq \mathbb{R}^n$ be a bounded domain and $\tau > n - 1$ be a fixed parameter. There exists a critical threshold $\varepsilon_0 = \varepsilon_0(H_1, \Omega; \mathbf{a}) > 0$ such that for any $0 < \varepsilon \leq \varepsilon_0$, the following properties hold:

1. **Measure of resonance:** There exists two small Lebesgue measure $\kappa = \kappa(n, \tau, \Omega) > 0$ and $\delta = \delta(\varepsilon) > 0$, where $\delta \rightarrow 0$ as $\varepsilon \rightarrow 0$, such that the excluded set of “bad” frequencies Ω^* satisfies $\text{mes}(\Omega^*) \leq \kappa + \delta$.
2. **Iterative sequence:** For any initial frequency $\boldsymbol{\omega}^{(0)} \in \Omega \setminus \Omega^*$ and initial lattice vector $\widehat{\mathbf{z}}^{(0)}$ defined in (2.6), the alternating numerical procedure, comprising the frequency update (2.19) and the non-resonant vector update (2.22), generates a sequence of iterates $\{(\boldsymbol{\omega}^{(r)}, \widehat{\mathbf{z}}^{(r)})\}_{r=0}^\infty$.
3. **Convergence:** There exists a Gevrey exponent $s = s(\varepsilon)$ such that this sequence remains within the product space $(\Omega \setminus \Omega^*) \times \mathcal{K}(s)$ and converges to the exact solution pair $(\boldsymbol{\omega}^*, \mathbf{z}^*)$.
4. **A priori estimates:** The convergence is characterized by the following error bounds:

$$\left\{ \begin{array}{l} \|\widehat{\mathbf{z}}^{(r)} - \widehat{\mathbf{z}}^*\| \leq \exp\left\{-\frac{3}{2}(M^s)^r\right\}, \\ |\boldsymbol{\omega}^{(r)} - \boldsymbol{\omega}^*| \leq \exp\left\{-\frac{3}{2}(M^s)^r\right\}. \end{array} \right. \quad (2.25a)$$

$$\left\{ \begin{array}{l} \|\widehat{\mathbf{z}}^{(r)} - \widehat{\mathbf{z}}^*\| \leq \exp\left\{-\frac{3}{2}(M^s)^r\right\}, \\ |\boldsymbol{\omega}^{(r)} - \boldsymbol{\omega}^*| \leq \exp\left\{-\frac{3}{2}(M^s)^r\right\}. \end{array} \right. \quad (2.25b)$$

Furthermore, for any $t \in [0, N_r]$, the approximate solution $\mathbf{z}^{(r)}(t)$ satisfies the time-domain error bound:

$$\|\mathbf{z}^{(r)}(t) - \mathbf{z}^*(t)\| \leq \exp\{-(M^s)^r\}. \quad (2.26)$$

This implies that as $r \rightarrow \infty$, the numerical solution $\mathbf{z}^{(r)}(t)$ converges to the exact quasi-periodic solution $\mathbf{z}^*(t)$ for any $t \geq 0$.

While the main theorem is established in ℓ_2 , the result extends to more compact Gevrey spaces. For any $s' \in [0, s)$, we define the norm

$$\|\widehat{\mathbf{z}}\|_{s'} = \left(\sum_{\mathbf{k} \in \mathbb{Z}^n} \|\widehat{\mathbf{z}}(\mathbf{k})\|^2 \exp\{|\mathbf{k}|^{2s'}\} \right)^{\frac{1}{2}}$$

The proof remains essentially unchanged in this setting. Moreover, this regularity can be generalized to the analytic setting. Let $\vartheta = \vartheta(\varepsilon)$ be an analytic strip that depends on the perturbation parameter. For any $\vartheta' \in [0, \vartheta)$, we define the analytic norm and the analytic decay condition as:

$$\|\widehat{\mathbf{z}}\|_{\vartheta'} = \left(\sum_{\mathbf{k} \in \mathbb{Z}^n} \|\widehat{\mathbf{z}}(\mathbf{k})\|^2 \exp\{2\vartheta'|\mathbf{k}|\} \right)^{\frac{1}{2}} \quad \text{and} \quad \sup_{\mathbf{k} \in \mathbb{Z}^n} (\|\widehat{\mathbf{z}}(\mathbf{k})\| \exp\{\vartheta|\mathbf{k}|\}) \leq 1.$$

¹Technically, this bound may be any positive constant; for convenience, we set it to 1 without loss of generality.

Theorem 2.2 remains valid in this setting as well. The proof of this theorem is established in Section 6, supported by the technical foundations laid in Section 4 and Section 5; a comprehensive outline of the proof strategy is provided Section 3.

Remark 2.3. The convergence bounds (2.25a) and (2.25b) represent a significant conceptual departure from classical KAM theory [Arnold, 1963, Moser, 1962]. While classical theory treats action variables as regular perturbations to preserve invariant tori, the present framework explicitly accounts for frequency drift in the existence of quasi-periodic solutions. Unlike standard KAM results, these estimates here incorporate a refined decay property of the Fourier coefficients, interpreting the solution's regularity itself as a singular perturbation [Witelski and Bowen, 2009]. The iteration lemma (Theorem 6.2) hinges on the super-exponential convergence of the vector field; consequently, the exponent s is not arbitrary. As the perturbation parameter vanish ($\varepsilon \rightarrow 0$), the exponent must vanish ($s \rightarrow 0$) at a rate faster than any polylogarithmic function of $1/\varepsilon$. In this regime, the admissible regularity becomes “almost zero”, restricting the solution's regularity nearly to ℓ_2 . This leads to a significant qualitative insight: even if the initial state $\hat{\mathbf{z}}^{(0)}$ possesses high regularity, the limiting state $\hat{\mathbf{z}}^*$ is necessarily confined to a low-regularity class. Theorem 2.2 remains valid in the analytic setting via the same inductive estimation strategy, provided that the strip width shrinks to zero ($\vartheta \rightarrow 0$) as $\varepsilon \rightarrow 0$. Finally, the convergence threshold $\varepsilon_0 = \varepsilon_0(H_1, \Omega, \mathbf{a})$ is fundamentally determined by the “input data” of the system, specifically the perturbation structure H_1 , the frequency set Ω , and the initial amplitude vector \mathbf{a} . For convenience, we assume $\varepsilon_0 \leq 1/2$ without loss of generality throughout the remainder of the paper.

3 Basic properties and conditions

The analysis in the following three sections is confined to the Gevrey decay set $\mathcal{K}(s)$ as defined in (2.24). In this initial section, we establish the basic properties necessary for the subsequent analysis. We then state the conditions required for the numerical implementation of the inverse of the tangent linear operator $T + \varepsilon B$, within the restricted lattice box Λ_N . Finally, we outline the overall strategy of the proof, with the technical details elaborated in Section 4 and Section 5.

3.1 Basic properties within the Gevrey decay set

Let $\mathbb{T}^n = [0, 2\pi]^n$ denote the n -dimensional torus. Recalling the vector field associated with the perturbation H_1 , we write down its Fourier coefficients as

$$\hat{\mathbf{X}}(\mathbf{k}) = \frac{1}{(2\pi)^n} \int_{\mathbb{T}^n} \frac{\partial H}{\partial \mathbf{z}} e^{-i\langle \mathbf{k}, \boldsymbol{\theta} \rangle} d\boldsymbol{\theta}, \quad (3.1)$$

for any $\mathbf{k} \in \mathbb{Z}^n$. Since the perturbation H_1 is a polynomial with real coefficients, we can characterize the regularity and boundedness of the resulting vector field within the Gevrey decay set.

Proposition 3.1. Suppose that the Fourier vector belongs to the Gevrey decay set as defined in (2.24), i.e., $\hat{\mathbf{z}} \in \mathcal{K}(s)$. Then there exists a constant $\gamma_1 = \gamma_1(H_1, s) > 0$ such that the components of the associated vector field satisfy

$$\sup_{\mathbf{k} \in \mathbb{Z}^n} \left(\|\hat{\mathbf{X}}(\mathbf{k})\| \exp \{|\mathbf{k}|^s\} \right) \leq \gamma_1. \quad (3.2)$$

Furthermore, there exists a constant $\gamma_2 = \gamma_2(H_1, s) > 0$ such that the vector fields satisfy the uniform bound:

$$\max \{ \|\widehat{\mathbf{X}}_q\|, \|\widehat{\mathbf{X}}_p\| \} \leq \|\widehat{\mathbf{X}}\| \leq \gamma_2. \quad (3.3)$$

The proof relies on the fact that the convolution operation preserves Gevrey decay properties (see Section A.2 for technical details). We now examine the entries of its tangent linear operators. By applying the Fourier expansion to the second-order derivative, we obtain the following kernels for any $\mathbf{k}, \mathbf{k}' \in \mathbb{Z}^n$:

$$\begin{cases} \mathcal{H}_1(\mathbf{k}, \mathbf{k}') = \frac{1}{(2\pi)^n} \int_{\mathbb{T}^n} \frac{\partial^2 H}{\partial \mathbf{z} \partial \mathbf{z}'} e^{-i\langle \mathbf{k} - \mathbf{k}', \theta \rangle} d\theta, \\ \mathcal{H}_2(\mathbf{k}, \mathbf{k}') = \frac{1}{(2\pi)^n} \int_{\mathbb{T}^n} \frac{\partial^2 H}{\partial \mathbf{z}^2} e^{-i\langle \mathbf{k} + \mathbf{k}', \theta \rangle} d\theta. \end{cases}$$

From these expressions, it follows that the kernels possess a Toeplitz-like and Hankel-like structures, respectively: $\mathcal{H}_1(\mathbf{k}, \mathbf{k}') = \mathcal{H}_1(\mathbf{k} - \mathbf{k}')$ and $\mathcal{H}_2(\mathbf{k}, \mathbf{k}') = \mathcal{H}_2(\mathbf{k} + \mathbf{k}')$. Consequently, the total tangent linear operator takes the form

$$\frac{\partial \widehat{\mathbf{X}}(\mathbf{k})}{\partial \widehat{\mathbf{z}}(\mathbf{k}')} = \mathcal{H}_1(\mathbf{k} - \mathbf{k}') + \mathcal{H}_2(\mathbf{k} + \mathbf{k}'). \quad (3.4)$$

Recall that $S = \partial \widehat{\mathbf{X}}_p / \partial \widehat{\mathbf{z}}_p$, introduced in (2.15), represents the non-resonant block of the tangent linear operator $\partial \widehat{\mathbf{X}}(\mathbf{k}) / \partial \widehat{\mathbf{z}}(\mathbf{k}')$. Following the decomposition $S = S_1 + S_2$, where the entries satisfy $S(\mathbf{k}, \mathbf{k}') = S_1(\mathbf{k} - \mathbf{k}') + S_2(\mathbf{k} + \mathbf{k}')$, its regularity and boundedness are characterized as follows.

Proposition 3.2. Assume $\widehat{\mathbf{z}} \in \mathcal{K}(s)$. There exist constants $\gamma_3, \gamma_4, \gamma_5 > 0$, depending on H_1 and s , such that the components of S satisfy:

$$\sup_{\mathbf{k}, \mathbf{k}' \in \mathcal{S}} (\|S_1(\mathbf{k} - \mathbf{k}')\| \exp \{|\mathbf{k} - \mathbf{k}'|^s\}) \leq \gamma_3 \quad (3.5a)$$

$$\sup_{\mathbf{k}, \mathbf{k}' \in \mathcal{S}} (\|S_2(\mathbf{k} + \mathbf{k}')\| \exp \{|\mathbf{k} + \mathbf{k}'|^s\}) \leq \gamma_4 \quad (3.5b)$$

Furthermore, the following uniform bound holds:

$$\max \left\{ \left\| \frac{\partial \widehat{\mathbf{X}}_q}{\partial \widehat{\mathbf{z}}_p} \right\|, \|S\| \right\} \leq \left\| \frac{\partial \widehat{\mathbf{X}}}{\partial \widehat{\mathbf{z}}} \right\| \leq \gamma_5. \quad (3.6)$$

Note that the entries $S_1(\mathbf{k} - \mathbf{k}')$ and $S_2(\mathbf{k} + \mathbf{k}')$ are $n \times n$ matrices; thus, the norm in (3.5) refers to the standard matrix norm, i.e., the largest singular value. Since $\partial \widehat{\mathbf{X}} / \partial \widehat{\mathbf{z}}$ and S are the real symmetric Hessian-type operators, the norms in (3.6) are understood in the spectral sense, i.e., the maximum absolute value of the eigenvalues. These results follow from Young's convolution inequality and the property that Gevrey decay is preserved under convolution. Detailed proofs are provided in Section A.3. We also require the regularity and boundedness properties for the frequency iteration operator B , as defined in (2.21).

Proposition 3.3. Assume $\widehat{\mathbf{z}} \in \mathcal{K}(s)$. There exist constants $\gamma_6, \gamma_7 > 0$ depending on H_1 and s , such that the components of B satisfy:

$$\sup_{\mathbf{k}, \mathbf{k}' \in \mathcal{S}} (\|B(\mathbf{k}, \mathbf{k}')\| \exp \{|\mathbf{k}|^s + |\mathbf{k}'|^s\}) \leq \gamma_6. \quad (3.7)$$

Furthermore, the following uniform bound holds:

$$\|B\| \leq \gamma_7. \quad (3.8)$$

The proof is provided in Section A.4. Finally, we bound the second-order derivative of the vector field generated by the perturbation H_1 , which constitutes a third-order tensor.

Proposition 3.4. Assume $\hat{\mathbf{z}} \in \mathcal{K}(s)$. There exist a constant $\gamma_8 = \gamma_8(H_1, s)$ such that

$$\max \left\{ \left\| \frac{\partial^2 \hat{\mathbf{X}}_q}{\partial \hat{\mathbf{z}}_p^2} \right\|, \left\| \frac{\partial S}{\partial \hat{\mathbf{z}}_p} \right\| \right\} \leq \left\| \frac{\partial^2 \hat{\mathbf{X}}}{\partial \hat{\mathbf{z}}^2} \right\| \leq \gamma_8. \quad (3.9)$$

The proof of Theorem 3.4 is provided in Section A.5. Let $\gamma = \max_{1 \leq j \leq 8} \gamma_j$, where each γ_j for $j = 1, \dots, 8$ depends on the perturbation Hamiltonian H_1 . By scaling H_1 , or, equivalently, by choosing a sufficiently small ε , we assume without loss of generality that $\gamma \leq 1/(2e) \leq 1/2$. Utilizing the estimates from Theorem 3.1, we establish the following result regarding the frequency drift.

Proposition 3.5. Assume $\hat{\mathbf{z}} \in \mathcal{K}(s)$. The frequency drift determined by the Q -equation (2.12) satisfies:

$$|\omega' - \omega| \leq \varepsilon. \quad (3.10)$$

and the Jacobian of the frequency map satisfies:

$$1 - \varepsilon \leq \left\| \frac{\partial \omega'}{\partial \omega} \right\|_2 \leq 1 + \varepsilon. \quad (3.11)$$

3.2 Conditions for efficient implementations

The heart of the alternating numerical procedure, as shown in Figure 4, lies in the update of the non-resonant vector via the dimension-enlarged Newton scheme (2.22). The major challenge in this approach is the ‘‘small-divisor’’ problem, which implies that the truncated matrix $(T + \varepsilon B)_N$ may become increasingly singular as the dimension N grows. To ensure an effective implementation, we must prevent the norm of the inverse truncation matrix from growing excessively. To quantify the allowable singularity and the required numerical precision, we define a size-dependent threshold parameter:

$$\varepsilon_N := \exp \{-(\log N)^{15}\}, \quad (3.12)$$

which serves as the error threshold for each truncation level N . In numerical practice, we evaluate the perturbed operator $T + \varepsilon B$ rather than T alone. The validity of the implementation depends on the following two conditions.

Condition 3.6 (Implementation Conditions). The truncated linearized operator $(T + \varepsilon B)_N$ must satisfy the following two conditions:

(1) **Inversion condition:** The operator norm of the inverse is bounded by the reciprocal of the size parameter:

$$\|(T + \varepsilon B)_N^{-1}\|_2 \leq \frac{1}{\varepsilon_N}. \quad (3.13)$$

(2) **Localization condition:** For sufficiently large spatial separations in the lattice Λ_N , specifically when $|\mathbf{k} - \mathbf{k}'| \geq N^{\frac{1}{2}}$ and $|\mathbf{k} + \mathbf{k}'| \geq N^{\frac{1}{2}}$ (denoted by $|\mathbf{k} \pm \mathbf{k}'| \geq N^{\frac{1}{2}}$ for short), the entries of the inverse matrix must exhibit Gevrey-type decay:

$$|(T + \varepsilon B)_N^{-1}(\mathbf{k}, \mathbf{k}')| \leq \exp\left\{-\frac{|\mathbf{k} - \mathbf{k}'|^s}{2}\right\} + \exp\left\{-\frac{|\mathbf{k} + \mathbf{k}'|^s}{2}\right\}. \quad (3.14)$$

Regarding the inversion condition in (3.13), we emphasize that all estimates are conducted using the ℓ_2 -norm. The localization condition (3.14) specified here refers to two-sided off-diagonal decay for lattice boxes centered at the origin $\mathbf{0}$. For “off-side” boxes of size N with centers $\mathbf{k}_0 \notin \Lambda_{2N}$, the distance $|\mathbf{k} + \mathbf{k}'| \geq 2N$ is always satisfied; consequently, we only need to consider the off-diagonal decay in terms of $|\mathbf{k} - \mathbf{k}'|$. The analysis presented in Section 4 and Section 5 focuses exclusively on the ℓ_2 -norm of the inverse and the localization of its entries for the operator $(T + \varepsilon B)$ restricted to off-side boxes. According, we postpone the detailed treatment of two-sided off-diagonal decay until Section 6.1. Furthermore, as these objectives do not require estimating the norm of the derivatives, the composite norm is unnecessary for these sections. We reserve its use for derivative estimates of the linear operator $(T + \varepsilon B)_N$, which are essential only for the Iteration Lemma (Theorem 6.2). For clarity and conciseness, the formal discussion of the composite norm is deferred to Theorem 6.1 in Section 6.2. Finally, note that the inclusion of the operator B in the numerical implementation renders the operator non-self-adjoint; therefore, the ℓ_2 -norm here corresponds to the largest singular value.

3.3 Outline of the inductive and multi-scale strategy

The proof of the main convergence statement (Theorem 2.2) follows a structural and multi-scale hierarchy. While the conceptual core of our approach remains rooted in the framework established by [Bourgain \[1998\]](#), our approach departs significantly in both presentation and execution. Guided by Theorem 3.6, we provide a more modular and transparent strategy as outlined below.

Small-scale preparation (Section 4) We begin by establishing foundational results for small-scale boxes to anchor the subsequent multi-scale analysis. Departing from the high-level techniques utilized by [Bourgain \[1998\]](#), we propose a significantly streamlined argument based on the Neumann series. Additionally, we clarify the relationship between the nearly-resonant set and the Diophantine condition common in classical KAM theory.

Multi-scale analysis (Section 5) This section streamlines the multi-scale analysis of [Bourgain \[1998\]](#), introducing a more efficient execution divided into two key components:

- Clustering of singular boxes (Section 5.1). We demonstrate how the second Melnikov condition effectively controls the diffusion of resonant clusters. Our simplified approach provides a more transparent bound on the complexity of these clusters.
- Multi-scale induction (Section 5.2). Using the small-box results as inductive bases, we employ the resolvent identity to derive a clear inductive step. We show that as long as the inversion

condition (3.13) holds, the localization condition (3.14) is naturally satisfied. This refinement reconstructs the logical progression explicitly, bypassing the dense, non-linear algebraic burdens typically associated with inductive resolvent bounds [Bourgain, 1998].

Furthermore, we demonstrate that the second Melnikov condition is not omitted rather localized. In finite dimensions, this corresponds directly to the classical the second Melnikov condition. This localized implementation is vital for PDE applications, such as the wave equation, which we explore in our forthcoming work.

Inductive Iteration and Completion (Section 6) The formal verification for Theorem 3.6 is conducted in Section 6.1, with specific focus on two-sided off-diagonal decay and the exclusion of “bad” frequencies. We restrict the linear operator to the lattice boxes with centers at the origin and compute its inverse as the dimension is incrementally expanded toward infinity. In Section 6.2, we establish Theorem 6.2 via rigorous inductive estimates, which serves as the final bridge to complete the convergence proof for our numerical algorithms.

Numerical experiments (Section 7) Finally, we demonstrate the efficiency of our approach using the Duffing equation and the Hénon-Heiles model. We highlight two key advantages over traditional methods. Our method provides precise approximations of frequencies and Fourier coefficients where standard symplectic integrators reach their limits. While symplectic algorithms conserve the symplectic form, they often fail to track precise pointwise positions over long time scales due to phase drift. Our multi-scale inductive approach ensures both structural stability and superior accuracy in predicting the exact state of the system at any given time.

4 Restricted operators on small boxes

From this section onward, we analyze the restricted operator $(T + \varepsilon B)_N$ as it arises within the dimension-enlarged Newton scheme (2.22). Specifically, our main objective is to establish the conditions under which this operator satisfies Theorem 3.6. In the iterative scheme (2.22), the reference box size at the r -th step is set as $N_{r+1} = M^{r+1}$. To establish the benchmark for scale separation, we determine the specific value of M relative to the perturbation parameter ε as:

$$M = \exp \left\{ \left(\log \frac{1}{\varepsilon} \right)^{\frac{1}{20}} \right\} \quad (4.1)$$

Based on the scaling factor M , we categorize the restricted lattice boxes defined in (2.16) into two distinct regimes:

- **Small restricted boxes.** The box size N falls within the range

$$M_0 = \exp \left\{ (\log M)^{\frac{1}{20}} \right\} \leq N \leq M. \quad (4.2)$$

In this regime, the dynamics are characterized by low-frequency oscillations or slow rotations.

- **Large restricted boxes** The box size satisfies

$$N > M, \quad (4.3)$$

where the dynamics here involves high-frequency oscillation or rapid rotations.

This section focuses exclusively on small restricted boxes. The analysis of large restricted boxes involves a more complex multi-scale approach, which is deferred to Section 5.

4.1 Nearly-resonance sets

The presence of “bad” frequencies typically gives rise to small-divisor problems, which may render the restricted operator non-invertible. To characterize such frequencies explicitly, we introduce the nearly-resonant set associated with a finite lattice box $\Lambda_{2(N+1)}$.

Definition 4.1. Let $\Omega \subseteq \mathbb{R}^n$ be a bounded domain. The *nearly-resonant set* associated with the restricted box $\Lambda_{2(M+1)}$ is defined as

$$\Omega_M^\tau = \left\{ \omega \in \Omega \mid |\langle \mathbf{k}, \omega \rangle| < \frac{1}{|\mathbf{k}|^\tau}, \mathbf{k} \in \Lambda_{2(M+1)} \setminus \{0\} \right\}. \quad (4.4)$$

The complement, $\Omega \setminus \Omega_M^\tau$, corresponds to the classical Diophantine condition used in KAM theory (see, e.g., [Arnold et al. \[2006\]](#)). Here, it serves to exclude “bad” frequencies within the small boxes. In the case of lower-dimensional quasi-periodic solutions, the nearly-resonant set naturally decomposes into two components corresponding to the first and second Melnikov conditions: the former, associated with the original small box, identifies “bad” frequencies that cause the operator’s eigenvalues to vanish (see Section 4.2), and the latter, arising from small translated boxes, addresses “difference resonances”. In this scenario, even if a singular eigenvalue may exist, all other eigenvalues of the translated block remain well-behaved. Consequently, if we can ensure that the singular eigenvalue remains “good”, then the inverse and its off-diagonal entries satisfy Theorem 3.6 (see Section 4.3). Further results concerning lower-dimensional quasi-periodic solutions will be presented in forthcoming work. The following lemma summarizes the measure estimates for these excluded (small-divisor) frequency sets.

Lemma 4.2. Let $\tau > n - 1$ be a fixed exponent. Then there exist a constant $\kappa = \kappa(n, \tau, \Omega) > 0$, depending on the dimension n , the domain Ω , and the parameter τ , such that the nearly-resonance set satisfies

$$\text{mes}(\Omega_M^\tau) \leq \kappa. \quad (4.5)$$

The proof relies only on elementary measure estimates and the convergence of a simple lattice sum, and is therefore deferred to Section B.1.

Remark 4.3. Beyond the analysis of the small boxes, the Melnikov conditions can be interpreted more deeply within the multi-scale analysis framework (see Section 5):

- **Single-box dynamics:** The first Melnikov condition is viewed as a single-box eigenvalue problem. It excludes frequency measures where the restricted operator fails to be “gap-broadening” or invertible.
- **Inter-box interactions:** The second Melnikov condition governs the interaction between two distinct boxes (or box translations). It ensures that resonance does not “propagate” or couple across different spatial locations.

A fundamental departure from classical KAM theory, where infinite-dimensional holomorphic equations require both Melnikov conditions to be satisfied simultaneously at every iteration, is the hierarchical application of these conditions. In the multi-scale analysis, based on a finer decomposition

of Fourier modes, these conditions are imposed progressively scale by scale. This relaxation constitutes a cornerstone of [Bourgain \[2005\]](#), allowing the treatment of higher-dimensional PDEs where frequency clusters would otherwise violate the standard (global) second Melnikov condition.

4.2 Restriction to the original small box

Excluding the set Ω_M^τ of the “bad” frequencies, we now analyze the inverse of the restricted operators within the small-size regime specified in (4.2). We begin by focusing on the operator restricted to the original box Λ_N .

Theorem 4.4. Assume that $\hat{\mathbf{z}} \in \mathcal{K}(s)$. If the frequency satisfies $\omega \in \Omega \setminus \Omega_M^\tau$, then the restricted operator T_N is invertible, and its inverse satisfies the operator norm bound

$$\|(T + \varepsilon B)_N^{-1}\|_2 \leq \frac{1}{\varepsilon_N}. \quad (4.6)$$

In addition, for any $\mathbf{k} \neq \pm\mathbf{k}' \in \Lambda_N$, the two-sided off-diagonal entries satisfy the Gevrey decay estimate:

$$|(T + \varepsilon B)_N^{-1}(\mathbf{k}, \mathbf{k}')| \leq \frac{1}{2} (\exp\{-|\mathbf{k} - \mathbf{k}'|^s\} + \exp\{-|\mathbf{k} + \mathbf{k}'|^s\}). \quad (4.7)$$

Given that $\hat{\mathbf{z}} \in \mathcal{K}(s)$, Theorem 3.5 implies that the drifted frequency ω' satisfies (3.10). For the diagonal operator D_N , its eigenvalues admit the uniform lower bound:

$$\begin{aligned} |D_{N;j,\mathbf{k}}| &\geq |-\langle \mathbf{k}, \omega \rangle + \omega_j| - |\langle \mathbf{k}, \omega' - \omega \rangle| \\ &\geq \frac{1}{n^\tau(N+1)^\tau} - N \exp\{-(\log M)^{20}\} \geq \frac{1}{2n^\tau(N+1)^\tau}, \end{aligned} \quad (4.8)$$

for any $j = 1, \dots, n$ and $-\mathbf{k} + \mathbf{e}_j \in \Lambda_N \setminus \{0\}$. This lower bound ensures that the diagonal part of the operator remains sufficiently far from zero, preventing singular behavior. Consequently, the inverse of the restricted operator T_N can be estimated via a Neumann series. Since the off-diagonal terms involve only convolution operations that interact predictably with the Gevrey decay, the detailed argument follows standard procedures and is therefore deferred to Section B.2.

4.3 Restriction to a translated small box

In this section, we analyze the behavior of the operator $T + \varepsilon B$ when restricted to a translated small box. For any fixed $\mathbf{k}_0 \in \mathbb{Z}^n \setminus \{0\}$, the translated box is defined as $\mathbf{k}_0 + \Lambda_N$. This spatial

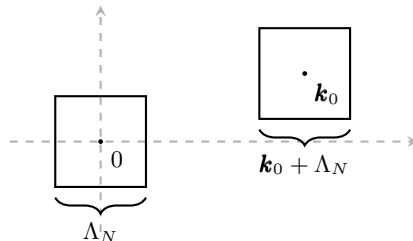


Figure 5: The original small box Λ_N and its translated counterpart $\mathbf{k}_0 + \Lambda_N$.

translation shifts the index set of the operator, as illustrated in Figure 5. We denote the restriction of the operator $T + \varepsilon B$ to this translated domain as

$$(T + \varepsilon B)_{\mathbf{k}_0, N} := (T + \varepsilon B)|_{\mathbf{k} \in \mathbf{k}_0 + \Lambda_N}. \quad (4.9)$$

Our analysis focuses on cases where the box center lies outside the region Λ_{2N} (i.e., $\mathbf{k}_0 \notin \Lambda_{2N}$). To evaluate this restricted operator, we recall the properties of the operator B defined in (2.21), which was constructed via a numerical algorithm to facilitate frequency updates. According to Theorem 3.3, the operator B exhibits double-index Gevrey decay. This property ensures that the norm of the restricted operator satisfies a Gevrey-type bound:

$$\|B_{\mathbf{k}_0, N}\| \leq (2N)^n \exp\{-N^s\}$$

for any $\mathbf{k}_0 \notin \Lambda_{2N}$. In practical terms, this estimate implies that the contribution of $B_{\mathbf{k}_0, N}$ is negligible compared to any scale involving exp-polylogarithmic decay, such as $\exp(-(\log N)^\nu)$ for $\nu > 0$. In other words, since Gevrey decay (with $s > 0$) is significantly faster than these scales, the additional operator B do not exert any meaningful influence on the spectral analysis within this regime.

To bound the inverse of $T_{\mathbf{k}_0, N}$, we introduce the shifted resonance parameter $\sigma_0 = -\langle \mathbf{k}_0, \boldsymbol{\omega}' \rangle$. This allows us to express the restricted operator as a spectral shift of T_N :

$$T_{\mathbf{k}_0, N} = \sigma_0 + T_N, \quad (4.10)$$

which we denote more concisely as $T_N^{\sigma_0}$. Since the operator S is translationally invariant, the translation acts exclusively on the diagonal component, such that $D_N^{\sigma_0} = D_{\mathbf{k}_0, N}$. By invoking Theorem 4.4, we ensure that for all $\boldsymbol{\omega} \in \Omega / \Omega_M^\tau$ and $\hat{\mathbf{z}} \in \mathcal{K}(s)$, the entries of $D_{N; j, \mathbf{k}}$ satisfy the lower bound established in (4.8). Following Theorem 4.1 regarding the non-resonant set, we establish the following property.

Proposition 4.5. Assume that $\hat{\mathbf{z}} \in \mathcal{K}(s)$. If the frequency satisfies $\boldsymbol{\omega} \in \Omega \setminus \Omega_N^\tau$, the diagonal operator $D_N^{\sigma_0}$ admits at most one index $\mathbf{k} \in \Lambda_N$ such that this diagonal entry $D_{N; j, \mathbf{k}}^{\sigma_0} = -\sigma_0 - \langle \mathbf{k}, \boldsymbol{\omega}' \rangle + \omega_j$ has an absolute value smaller than $(4n)^{-\tau}(N+1)^{-\tau}$.

The proof follows the same argument presented in Section 4.2 and is therefore deferred to Section B.3. In light of Theorem 4.5, we define the unique index (if it exists) as the singular index \mathbf{k}_* , and its corresponding value $\sigma_* = -\langle \mathbf{k}_*, \boldsymbol{\omega}' \rangle$ as the *minimal resonance gap* (or *minimal shift*). Consequently, the singular site is defined as the singleton set $\Pi = \{\mathbf{k}_*\}$. To maintain consistency with the subsequent multi-scale analysis, we re-index the small box as $\Xi_0 = \mathbf{k}_0 + \Lambda_N$. By applying a Neumann series and proceeding analogously to Theorem 4.4, we can reformulate Theorem 4.5 into the following lemma for the non-resonant index set $\Xi_0 \setminus \Pi$, which serves as the inductive base for the multi-scale induction in Section 5.2.

Lemma 4.6. Assume that $\hat{\mathbf{z}} \in \mathcal{K}(s)$ and $\boldsymbol{\omega} \in \Omega \setminus \Omega_M^\tau$. For any center $\mathbf{k}_0 \notin \Lambda_{2(N+1)}$, then the restricted operator $(T + \varepsilon B)|_{\Xi_0 \setminus \Pi}$ is invertible, and its inverse satisfies the operator norm bound

$$\|((T + \varepsilon B)|_{\Xi_0 \setminus \Pi})^{-1}\|_2 \leq (4n)^\tau(N+1)^\tau. \quad (4.11)$$

In addition, the off-diagonal entries of $((T + \varepsilon B_N)|_{\Xi_0 \setminus \Pi})^{-1}$ satisfy the decay estimate

$$|((T + \varepsilon B)|_{\Xi_0 \setminus \Pi})^{-1}(\mathbf{k}, \mathbf{k}')| \leq \exp\{-|\mathbf{k} - \mathbf{k}'|^s\}, \quad (4.12)$$

for any $\mathbf{k} \neq \mathbf{k}' \in \Xi_0 \setminus \Pi$.

For small translated boxes, the inversion condition (3.13) can be verified by examining the diagonal operator alone. Since the perturbation parameter is assumed to satisfy $\varepsilon \ll \varepsilon_N$, the control of the diagonal operator's entries is already well-separated from the resonance. Specifically, if the minimal resonant gap satisfies $|\sigma_\star + \omega_j| \geq \varepsilon_N$ for $j = 1, \dots, n$, then we establish the restricted operator on a translated box satisfies the localization condition (3.14)

Theorem 4.7. Assume that $\hat{\mathbf{z}} \in \mathcal{K}(s)$ and $\boldsymbol{\omega} \in \Omega \setminus \Omega_M^\tau$. For any $\mathbf{k}_0 \notin \Lambda_{2(N+1)}$, if the minimal resonant gap satisfies $|\sigma_\star + \omega_j| \geq \varepsilon_N$, then the restricted operator $(T + \varepsilon B)_{\mathbf{k}_0, N}$ is invertible, and its inverse satisfies the operator norm bound

$$\|(T + \varepsilon B)_{\mathbf{k}_0, N}^{-1}\|_2 \leq \frac{1}{\varepsilon_N}. \quad (4.13)$$

In addition, the off-diagonal entries of T_N^{-1} satisfy the decay estimate

$$\left| (T + \varepsilon B)_{\mathbf{k}_0, N}^{-1}(\mathbf{k}, \mathbf{k}') \right| \leq \exp\{-|\mathbf{k} - \mathbf{k}'|^s\}, \quad (4.14)$$

for any $\mathbf{k} \neq \mathbf{k}' \in \mathbf{k}_0 + \Lambda_N$.

While Theorem 4.6 may seem redundant for the small-box regime specified in (4.2), it serves two primary purposes: first, it characterizes the behavior at the smallest scale of our multi-scale analysis; and second, it provides the necessary inductive basis for that analysis. The transitions from Theorem 4.5 to Theorem 4.6, and subsequently from Theorem 4.6 to Theorem 4.7, are achieved via the resolvent identity, as demonstrated in Section 5.2.

5 Multi-scale analysis: extension to large boxes

In this section, we extend our analysis to restricted large boxes of size $N > M$, centered at $\mathbf{k}_0 \notin \Lambda_{2N}$. To control the propagation of resonances across these expanding scales, we employ a hierarchical exclusion process. This method, fundamentally established by Bourgain [1994, 1998], involves the iterative removal of “bad” frequencies that trigger small divisors. Below, we present a streamlined version of this technique, focusing on the systematic refinement of the non-resonant set.

5.1 Size reduction: clustering of singular boxes

To bridge the operator properties across disparate scales, we introduce a reduced scale N' derived from the larger scale N via the following polylogarithmic scaling:

$$N' = \exp\left\{(\log N)^{\frac{1}{10}}\right\}. \quad (5.1)$$

This specific scaling allows us to isolate resonant interactions by identifying parameters where the small divisors, specifically those involving the frequency difference, fall below a critical threshold.

Definition 5.1. The *difference nearly-resonant set* is defined as:

$$\Omega_{2,N} = \left\{ \boldsymbol{\omega} \in \Omega \mid |-\langle \mathbf{k}, \boldsymbol{\omega}' \rangle + \omega_{j_1} - \omega_{j_2}| < 4\varepsilon_{N'}, \forall \mathbf{k} \in \Lambda_{2N} \setminus \Lambda_{2N'}, \forall j_1, j_2 = 1, \dots, n \right\}. \quad (5.2)$$

The *total difference nearly-resonant set* is subsequently as the union over all scales $N > M$:

$$\Omega_2 = \bigcup_{N > M} \Omega_{2,N}.$$
 (5.3)

Under the assumption that the frequency satisfies $\omega \notin \Omega_{2,N}$, we analyze the behavior of all smaller boxes of size N' contained within the larger box of size N . We can ensure that if the operator $T + \varepsilon B$ restricted to these smaller boxes violates the inversion condition (3.13), then the centers of these singular boxes must be clustered. Specifically, their centers are located within a distance of $4N'$, as illustrated in Figure 6.

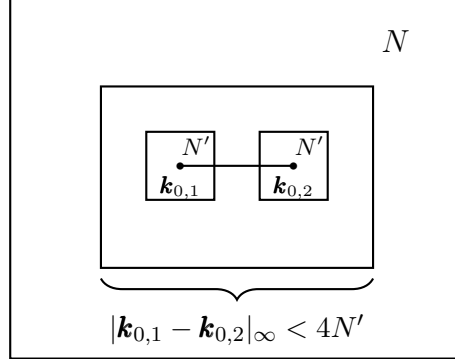


Figure 6: The clustering of singular box centers as the size reduction.

Next, we provide a formal justification for the clustering phenomenon described above. Consider two small boxes with centers $\mathbf{k}_{0,1}, \mathbf{k}_{0,2} \in \mathbf{k}_0 + \Lambda_N$. Given that the frequency satisfies $\omega \notin \Omega_{2,N}$, the entries of the diagonal operators, $D_{\mathbf{k}_{0,1}, N'}$ and $D_{\mathbf{k}_{0,2}, N'}$, must be sufficiently distinct for any $|\mathbf{k}_{0,1} - \mathbf{k}_{0,2}|_{\infty} \geq 4N'$. Owing to the smallness of the operator B (introduced in the numerical update) and the translational invariance of the nonlinear perturbation operator S , we can bound the difference between the smallest singular values of the restricted operators $T_{\mathbf{k}_{0,1}, N'}$ and $T_{\mathbf{k}_{0,2}, N'}$. Specifically, we establish the following estimate:

$$|\min s(T + \varepsilon B)_{\mathbf{k}_{0,1}, N} - \min s(T + \varepsilon B)_{\mathbf{k}_{0,2}, N}| \geq 3\varepsilon_{N'} \quad (5.4)$$

which demonstrates that if both boxes are “singular” (i.e., their smallest singular values are small), they cannot be far apart. To formalize this spatial clustering, we define $\Sigma(\mathbf{k}_0, N)$ as the set of box centers within the larger domain $\mathbf{k}_0 + \Lambda_N$ that violates the inversion condition (3.13)

$$\Sigma(\mathbf{k}_0, N) = \left\{ \mathbf{k}'_0 \in \mathbf{k}_0 + \Lambda_N, \mathbf{k}_0 \notin \Lambda_{2N} \left| \|(T + \varepsilon B)_{\mathbf{k}'_0, N'}^{-1}\|_2 > \frac{1}{\varepsilon_{N'}} \right. \right\}. \quad (5.5)$$

We then rigorously characterize the spatial clustering of these singular centers with the following lemma.

²The subscript “2” identifies the nearly-resonant set associated with the second Melnikov condition in classical KAM theory. Its localized interpretation is briefly noted in Theorem 5.3, while its wider applications are explored in our forthcoming work. In contrast, the subscript “1” refers to the single-mode nearly-resonant set (first Melnikov condition). The procedure for excluding “bad” frequencies and its multi-scale extension are detailed in Section 5.3.

Lemma 5.2. Assume that $\hat{\mathbf{z}} \in \mathcal{K}(s)$ and $\boldsymbol{\omega} \in \Omega \setminus (\Omega_M^\tau \cup \Omega_{2,N})$. If a box center satisfies $\mathbf{k}'_0 \in \Sigma(\mathbf{k}_0, N)$, then it must be located within a small box of radius $4N'$:

$$\mathbf{k}'_0 \in \mathbf{k}''_0 + \Lambda_{4N'}$$

where $\mathbf{k}''_0 \in \mathbf{k}_0 + \Lambda_N$.

Remark 5.3. As demonstrated above, the total difference nearly-resonant set corresponds to the second Melnikov condition, specifically regarding the persistence of low-dimensional tori. However, this construction marks a pivotal departure from classical KAM theory. Unlike classical theory, which relies on a uniform, “all-at-once” exclusion of resonant sets from the outset, the difference nearly-resonant set is excluded incrementally as the box size N increases. This iterative exclusion necessitates the multi-scale analysis, distinguishing it from standard KAM techniques adapted for the PDE setting (see [Kuksin, 2000, Liu and Yuan, 2011, Yuan, 2021]). When infinite-dimensional “normal” frequencies arise from spatial Fourier decomposition, their influence is inherently localized rather than global, being determined by their specific magnitudes and directions. As captured by Bourgain [2005], accounting for such localized interactions is essential for the rigorous analysis of high-dimensional PDEs, particularly those involving multiple identical parameters or repeated eigenvalues (multiplicity), which is further exploited in our forthcoming work.

5.2 Multi-scale induction: inversion implies localization

Following the reduction scheme established in Section 5.1, the initial large box is iteratively scaled down to a size $4N'$, where $M_0 \leq N' \leq M$ and $M_0 \leq 4N' \leq M$. This process generates a nested sequence of boxes, an “onion-like” hierarchy, where each layer is strictly contained within the previous one. The structure relies on the interplay between resonance and inversion across scales. By Theorem 4.5, each such small box in this sequence is guaranteed to contain at most one minimal resonance gap $\sigma_\star = \langle \mathbf{k}_\star, \boldsymbol{\omega}' \rangle$. Simultaneously, for each box centered in the intermediate (annular) region, Theorem 5.2 ensures that the restricted operator satisfies the inversion condition (3.14). Importantly, this nested configuration is inherited by the sub-boxes within the intermediate regions, thereby preserving structural uniformity across all scales. This multiscale reduction is categorized into three distinct sets:

- **Resonant boxes:** The sequence of boxes containing the singular sites Π :

$$\mathbf{k}_0 + \Lambda_N = \Xi_{J+1} \supset \Xi_J \supset \dots \supset \Xi_0 \supset \Pi,$$

where the scale is defined by $|\Xi_j| = 4N_j$ for $j = 0, \dots, J$.

- **Intermediate sub-boxes:** The boxes located within the region $\Xi_{j+1} \setminus \Xi_j$, denoted as Γ_j , each of fixed size N_j .
- **Non-resonant index sets:** The sets of indices excluding the singular site are defined as $\Upsilon_j = \Xi_{j+1} \setminus \Pi$ for $t = -1, 0, \dots, J$.

The spatial relationship between the resonant box chain, the non-resonant intermediate sub-boxes, and the singular site is shown in Figure 7.

With these preparations above, we now state the following theorem for the multi-scale analysis, which extends the results obtained for small boxes (Theorem 4.7) to larger scales via induction.

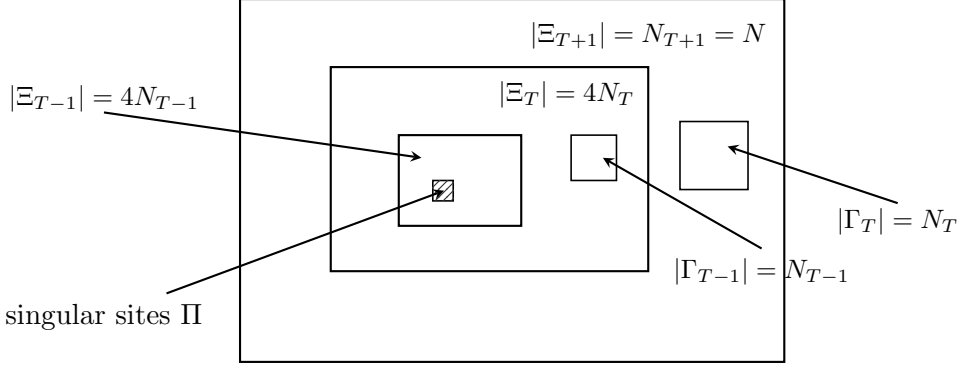


Figure 7: The multiscale box reduction process. The large-scale box Λ_N is organized into a resonant chain Ξ_t (containing the singular site Π) coupled with a collection of non-resonant sub-boxes Γ_t . This hierarchical structure forms the basis for proving the localization of the inverse operator.

Theorem 5.4. Assume that $\hat{\mathbf{z}} \in \mathcal{K}(s)$ and $\omega \in \Omega \setminus (\Omega_M^\tau \cup G)$. Suppose for any $M^0 \leq N \leq M^r$, the operator $(T + \varepsilon B)_N$ satisfies Theorem 3.6. If the inversion condition (3.13) is satisfied for any $M^r < N \leq M^{r+1}$, then the localization condition

$$|(T + \varepsilon B)_{\Xi_{j+1}}^{-1}(\mathbf{k}_1, \mathbf{k}_2)| \leq \exp \left\{ -\frac{|\mathbf{k}_1 - \mathbf{k}_2|^s}{2} \right\}, \quad \text{for } |\mathbf{k}_1 - \mathbf{k}_2| > N_{j+1}^{\frac{1}{2}} \quad (5.6)$$

is also satisfied for the same range.

Following the multi-scale reduction (Theorem 5.2) and the notations provided above, we now proceed with the proof. In direct correspondence with the small box analysis for the size range specified in (4.2) (see Section 4.3), the proof is organized into the following two steps.

Non-resonant gluing For the base case ($i = 0$), we consider the inverse operator $(T + \varepsilon B)_{\Upsilon_{-1}}^{-1} = (T + \varepsilon B)_{\Xi_0 \setminus \Pi}^{-1}$. The non-resonant index set $\Upsilon_{-1} = \Xi_0 \setminus \Pi$ and its corresponding inverse were previously constructed in Theorem 4.6. Given the small box size specified in the regime (4.2), the operator satisfies both the norm bound (4.11) and the off-diagonal decay estimates (4.12), thereby establishing the initial step.

We now invoke the inductive hypothesis for the step $i = j$. By construction, the non-resonant index sets Υ_{j-1} and the intermediate sub-boxes Γ_j satisfy both the inversion condition (4.13) and the localization condition (4.14). To treat the larger set Υ_j , we apply the resolvent identity in block form. By decomposing the set as $\Upsilon_j = \Gamma_j \cup (\Upsilon_j \setminus \Gamma_j)$, we obtain the following identity:

$$(T + \varepsilon B)_{\Upsilon_j}^{-1} = \begin{pmatrix} (T + \varepsilon B)_{\Gamma_j}^{-1} & 0 \\ 0 & (T + \varepsilon B)_{\Upsilon_j \setminus \Gamma_j}^{-1} \end{pmatrix} - \begin{pmatrix} -(T + \varepsilon B)_{\Gamma_j}^{-1} & 0 \\ 0 & (T + \varepsilon B)_{\Upsilon_j \setminus \Gamma_j}^{-1} \end{pmatrix} \begin{pmatrix} 0 & \varepsilon P^* \\ \varepsilon P & 0 \end{pmatrix} (T + \varepsilon B)_{\Upsilon_j}^{-1} \quad (5.7)$$

where the operators P and P^* are coupling operators generated from $B + S$. In terms of matrix entries, this identity is expressed as:

$$(T + \varepsilon B)_{\Upsilon_j}^{-1}(\mathbf{k}_1, \mathbf{k}_2) = (T + \varepsilon B)_{\Gamma_j}^{-1}(\mathbf{k}_1, \mathbf{k}_2)$$

$$-\varepsilon \sum_{\mathbf{k}_3 \in \Gamma_j} \sum_{\mathbf{k}_4 \in \Upsilon_j \setminus \Gamma_j} (T + \varepsilon B)^{-1}_{\Gamma_j}(\mathbf{k}_1, \mathbf{k}_3) P^*(\mathbf{k}_3, \mathbf{k}_4) (T + \varepsilon B)^{-1}_{\Upsilon_j}(\mathbf{k}_4, \mathbf{k}_2) \quad (5.8)$$

where \mathbf{k}_1 is the center of an intermediate sub-box Γ_j . Following Theorem 3.2 and Theorem 3.3, since the lattice box center under consideration lies outside the box Λ_{2N} , the coupling operators exhibit Gevrey decay:

$$P(\mathbf{k}, \mathbf{k}') \leq \frac{2}{3} \exp \{-|\mathbf{k} - \mathbf{k}'|^s\}, \quad \text{and} \quad P^*(\mathbf{k}, \mathbf{k}') \leq \frac{2}{3} \exp \{-|\mathbf{k} - \mathbf{k}'|^s\}. \quad (5.9)$$

By substituting the Gevrey decay (5.9) into the resolvent identity (5.8), we derive two iterative inequalities based on the distance between indices:

- For any $|\mathbf{k}_1 - \mathbf{k}_2| \geq 2N_j^{\frac{1}{2}}$, the resolvent identity (5.8) reads:

$$\begin{aligned} |(T + \varepsilon B)^{-1}_{\Upsilon_j}(\mathbf{k}_1, \mathbf{k}_2)| &\leq \exp \{-|\mathbf{k}_1 - \mathbf{k}_2|^s\} \\ &\quad + \varepsilon \sum_{\mathbf{k}_4 \in \Upsilon_j \setminus \Gamma_j} \exp \left\{ -\frac{|\mathbf{k}_1 - \mathbf{k}_4|^s}{2} \right\} |(T + \varepsilon B)^{-1}_{\Upsilon_j}(\mathbf{k}_4, \mathbf{k}_2)| \end{aligned} \quad (5.10)$$

- For any $|\mathbf{k}_1 - \mathbf{k}_2| < 2N_j^{\frac{1}{2}}$, the resolvent identity (5.8) reads:

$$\begin{aligned} |(T + \varepsilon B)^{-1}_{\Upsilon_j}(\mathbf{k}_1, \mathbf{k}_2)| &\leq \exp \{(\log 4N_j)^{15}\} \\ &\quad + \varepsilon \sum_{\mathbf{k}_4 \in \Upsilon_j \setminus \Gamma_j} \exp \left\{ -\frac{|\mathbf{k}_1 - \mathbf{k}_4|^s}{2} \right\} |(T + \varepsilon B)^{-1}_{\Upsilon_j}(\mathbf{k}_4, \mathbf{k}_2)| \end{aligned} \quad (5.11)$$

By utilizing the iterative inequalities, (5.10) and (5.11), we establish the following L^1 and L^∞ bounds:

$$\left\{ \sum_{\mathbf{k}_1 \in \Upsilon_j} |(T + \varepsilon B)^{-1}_{\Upsilon_j}(\mathbf{k}_1, \mathbf{k}_2)| \leq \exp \{(\log N_j)^{16}\} + \sqrt{\varepsilon} \|(T + \varepsilon B)^{-1}_{\Upsilon_j}\|_1 \right. \quad (5.12a)$$

$$\left. \sum_{\mathbf{k}_2 \in \Upsilon_j} |(T + \varepsilon B)^{-1}_{\Upsilon_j}(\mathbf{k}_1 - \mathbf{k}_2)| \leq \exp \{(\log N_j)^{16}\} + \sqrt{\varepsilon} \|(T + \varepsilon B)^{-1}_{\Upsilon_j}\|_\infty \right. \quad (5.12b)$$

By taking the maximum of these bounds and applying the Schur test, we arrive at the operator norm estimate:

$$\|(T + \varepsilon B)^{-1}_{\Upsilon_j}\|_2 \leq \sqrt{\|(T + \varepsilon B)^{-1}_{\Upsilon_j}\|_1 \cdot \|(T + \varepsilon B)^{-1}_{\Upsilon_j}\|_\infty} \leq \exp \{(\log N_j)^{17}\}. \quad (5.13)$$

For any $|\mathbf{k}_1 - \mathbf{k}_2| > N_j$, the resolvent identity (5.8) implies

$$|(T + \varepsilon B)^{-1}_{\Upsilon_j}(\mathbf{k}_1, \mathbf{k}_2)| \leq \frac{\varepsilon}{2} \sum_{\mathbf{k}_4 \in \Upsilon_j \setminus \Gamma_j} \exp \left\{ -\frac{|\mathbf{k}_1 - \mathbf{k}_4|^s}{2} \right\} |(T + \varepsilon B)^{-1}_{\Upsilon_j}(\mathbf{k}_4, \mathbf{k}_2)|$$

Given that the inversion bound (5.13) holds, repeated application of this iteration yields the final localization bound:

$$|(T + \varepsilon B)^{-1}_{\Upsilon_j}(\mathbf{k}_1, \mathbf{k}_2)| \leq \frac{1}{2} \exp \left\{ -\frac{|\mathbf{k}_1 - \mathbf{k}_2|^s}{2} \right\}. \quad (5.14)$$

Inversion and localization Finally, for the regime where $|\mathbf{k}_1 - \mathbf{k}_2| > N_j$, the resolvent identity leads to the following refinement:

$$\begin{aligned} |(T + \varepsilon B)_{\Xi_{j+1}}^{-1}(\mathbf{k}_1, \mathbf{k}_2)| &\leq \frac{1}{2} \exp \left\{ -\frac{|\mathbf{k}_1 - \mathbf{k}_2|^s}{2} \right\} \\ &\quad + \frac{\sqrt{\varepsilon}}{2} \sum_{\mathbf{k}_4 \in \Xi_{j+1} \setminus \Upsilon_j} \exp \left\{ -\frac{|\mathbf{k}_1 - \mathbf{k}_4|^s}{2} \right\} |(T + \varepsilon B)_{\Xi_{j+1}}^{-1}(\mathbf{k}_4, \mathbf{k}_2)| \end{aligned}$$

Incorporating the inversion bound (4.13) to control the diagonal term and repeating application of the above iteration, we derive the final localization bound (5.6), which completes the proof of Theorem 5.4.

5.3 From small to large boxes: exclusion of resonant frequencies across scales

In this section, we establish the mechanism for excluding the “bad” frequencies (the resonant set) to ensure the validity of the inverse estimates required for Theorem 4.7 and Theorem 5.4. The strategy for measure exclusion shifts depending on the box size regime.

Small box regime For small boxes within regime (4.2), the perturbation parameter ε remains smaller than ε_N . In this context, a Neumann series approach, consistent with Theorem 4.4, is sufficient to maintain control over the operator. To ensure invertibility, we explicitly characterize the excluded frequencies via the single-mode resonant set:

$$\Omega_{1,N} = \{ \boldsymbol{\omega} \in \Omega \mid |\sigma_\star + \omega_j| = | - \langle \mathbf{k}_\star, \boldsymbol{\omega}' \rangle + \omega_j | < \varepsilon_N, \forall j = 1, \dots, n \}, \quad (5.15)$$

It follows by direct calculation that the measure of this set satisfies:

$$\text{mes}(\Omega_{1,N, \mathbf{k}_0}) \leq n^2 (2N + 1)^{n-1} \varepsilon_N. \quad (5.16)$$

Large box regime For large boxes defined in regime (4.3), we analyze the norm of the restricted operator, specifically its smallest singular value. We represent the operator $(T + \varepsilon B)_{\mathbf{k}_0, N}$ in a block structure partitioned by the singular site Π :

$$(T + \varepsilon B)_{\mathbf{k}_0, N} = \begin{pmatrix} (T + \varepsilon B)_{\Xi_{j+1} \setminus \Pi} & P_1^* \\ P_1 & (T + \varepsilon B)_\Pi \end{pmatrix}. \quad (5.17)$$

To analyze this structure, we introduce the Schur complement of $(T + \varepsilon B)_{\mathbf{k}_0, N}$ with respect to the singular site Π (see [Golub and Van Loan \[2013, Section 3.2.11\]](#))

$$U = (T + \varepsilon B)_\Pi - P_1 (T + \varepsilon B)_{\Xi_{j+1} \setminus \Pi}^{-1} P_1^* \quad (5.18)$$

where the operator restricted to the singular site is expressed as:

$$(T + \varepsilon B)_\Pi = \sigma_\star + \boldsymbol{\omega} + \varepsilon (S + B)(\mathbf{k}_\star, \mathbf{k}_\star) \quad (5.19)$$

Since $\|P_1^*\|$ and $\|P_1\|$ are both bounded by ε , we can control the inverse of $(T + \varepsilon B)_{\mathbf{k}_0, N}$ as

$$\left\| (T + \varepsilon B)_{\mathbf{k}_0, N}^{-1} \right\|_2 \leq 4 \left\| (T + \varepsilon B)_{\Xi_{j+1} \setminus \Pi}^{-1} \right\|_2^2 \cdot \|U^{-1}\|_2 + \left\| (T + \varepsilon B)_{\Xi_{j+1} \setminus \Pi}^{-1} \right\|_2. \quad (5.20)$$

If we can control $\|U^{-1}\|_2$ by $1/\sqrt{\varepsilon_N}$, then we have together with (5.13) that

$$\left\| (T + \varepsilon B)_{\mathbf{k}_0, N}^{-1} \right\|_2 \leq \frac{1}{\varepsilon_N}.$$

Therefore, we only need to focus on the Schur complement U . By substituting (5.19) into (5.18), we reformulate the Schur complement as $U = \sigma_\star + \Phi$, where the perturbation term collects the remaining terms:

$$\Phi = \boldsymbol{\omega} + \varepsilon(S + B)(\mathbf{k}_\star, \mathbf{k}_\star) - P_1(T + \varepsilon B)_{\Xi_{J+1} \setminus \Pi}^{-1} P_1^*. \quad (5.21)$$

Given the estimate $\|\Phi\|_2 \leq 2 \exp\{(\log N)^{17/10}\}$ as shown in (5.13), and applying the triangle inequality $\|\sigma_\star + \Phi\|_2 \geq |\sigma_\star| - \|\Phi\|_2$, we define the single-mode resonant set for the large box as

$$\Omega_{1,N} = \{\boldsymbol{\omega} \in \Omega \mid |\sigma_\star| - \|\Phi\|_2 < \varepsilon_N, \forall j = 1, \dots, n\}. \quad (5.22)$$

The exclusion of measure for the large box does not possess the simple structure found in the small box regime. Instead of approximating polynomials via the Malgrange Preparation Theorem and excluding measure through derivative estimates (as in [Bourgain, 1998]), we adopt a strategy based on the so-called Cartan estimates for analytic functions, as introduced by Bourgain [2005]. For our purposes, we utilize a simplified version from Levin [1996].

Lemma 5.5 (Theorem 4 of Lecture 11.3 in Levin [1996]). Let $f(x)$ be a function analytic in the disk $\{z : |z| \leq 2eR\}$, $|f(0)| = 1$, and let η be an arbitrary small positive number. Then the estimate

$$\log |f(z)| > -H(\eta) \log M_f(2eR), \quad H(\eta) = \log \frac{15e^3}{\eta},$$

is valid everywhere in the disk $\{z : |z| \leq R\}$ except a set disks (C_j) with sum of radii

$$\sum r_j \leq \eta R.$$

To complete the measure estimates, we consider the magnitude of the perturbation Φ in two separate regimes. Under the condition $\|\Phi\|_2 < \sqrt{\varepsilon_N}$, the resonant set is contained within:

$$\Omega_{1,N} \subseteq \{\boldsymbol{\omega} \in \Omega \mid |\sigma_\star| < 2\sqrt{\varepsilon_N}, \forall j = 1, \dots, n\}. \quad (5.23)$$

In this regime, the measure estimate follows directly from the volume of the resonant slabs:

$$\text{mes}(\Omega_{1,N, \mathbf{k}_0}) \leq 2n^2(2N+1)^{n-1}\sqrt{\varepsilon_N}. \quad (5.24)$$

When $\|\Phi\|_2 \geq \sqrt{\varepsilon_N}$, we define the analytic function as

$$f(\sigma_\star) = \frac{|\sigma_\star|}{\|\Phi\|_2} - 1 \quad (5.25)$$

with the disk parameter as $\|\Phi\|_2 = 2e(1+e)^{-1}R$. It follows that $|f(0)| = 1$ and $M_f(2eR) = e$. By setting $\eta = 15e^3\sqrt{\varepsilon_N}$, Theorem 5.5 implies the following measure estimate as

$$\text{mes}(\Omega_{1,N, \mathbf{k}_0}) \leq \text{mes}(\{\boldsymbol{\omega} \in \Omega \mid |f(\sigma_\star)| < \sqrt{\varepsilon_N}\}) \leq 8(1+e)e^2 \exp\{(\log N)^{17/10}\} \sqrt{\varepsilon_N}. \quad (5.26)$$

Combing the measure estimates (5.16), (5.24), and (5.26), we establish the measure for the “bad” frequencies as below.

Theorem 5.6. For any $N \geq M_0$ and any box of size N with center $\mathbf{k}_0 \notin \Lambda_{2N}$, there exist a threshold $\varepsilon_0 > 0$ such that for all $\varepsilon \in (0, \varepsilon_0]$, if the operator $T + \varepsilon B$ restricted to the box $\mathbf{k}_0 + \Lambda_N$ satisfy the inversion condition (4.13), then the measure of the “bad” frequencies set satisfies

$$\text{mes}(\Omega_{1,N,\mathbf{k}_0}) \leq \varepsilon_N^{\frac{1}{4}}. \quad (5.27)$$

6 Proof of the main theorem

In this section, we present the formal proof of the main statement. We begin in Theorem 3.6 by verifying Section 6.1 via the pave method and extending these results to the derivatives. Subsequently, Section 6.2 provides the inductive estimate. Finally, we apply the iteration lemma to complete the proof.

6.1 Verification of Theorem 3.6

We proceed by induction on the size N . Following Theorem 4.4 as the base case, which satisfies Theorem 3.6, we now consider the inverse operator T_N^{-1} for $M^r < N \leq M^{r+1}$. Assume the result holds for $M_0 \leq N \leq M^r$, we set the parameters $K = N^{1/10}$ and consider a central box with size $10K$. Let $\Gamma_\alpha = \mathbf{k}_{0,\alpha} + \Lambda_K$ to be a collection of boxes such that $\mathbf{k}_{0,\alpha} \notin \Lambda_{5K}$. The set Λ_N can then be decomposed as:

$$\Lambda_N = \Lambda_{10K} \bigcup \left(\bigcup_\alpha \Gamma_\alpha \right) \quad (6.1)$$

Since the total number of the lattice points in Γ_α is at most $(2K^{10} + 1)^n$, we apply Theorem 3.4 and Theorem 5.6 to estimate the single-mode nearly-resonant set. Specifically, by summing the measures of the “bad” frequencies associated with each localized box at scale K , we obtain:

$$\text{mes}(\Omega_{1,K}) \leq \sum_\alpha \text{mes}(\Omega_{1,K,\mathbf{k}_{0,\alpha}}) \leq (2K^{10} + 1)^n \varepsilon_K^{\frac{1}{4}}. \quad (6.2)$$

Thus, the total measure for the single-mode nearly-resonant set can be estimated by:

$$\text{mes}(\Omega_1) \leq \sum_{K=M_0}^{\infty} (2K^{10} + 1)^n \exp \left\{ \frac{(\log K)^{15}}{4} \right\}. \quad (6.3)$$

From Theorem 5.1, we can derive the total measure of the difference nearly-resonant set as:

$$\text{mes}(\Omega_2) \leq \sum_{K=M_0}^{\infty} (2K^{10} + 1)^n \exp \left\{ (\log K)^{\frac{3}{2}} \right\}. \quad (6.4)$$

Combining (6.3) and (6.4), we can choose the threshold $\varepsilon_0 > 0$ such that the total measure of “bad” frequencies, $\text{mes}(\Omega_1 \cup \Omega_2)$, is sufficiently small to satisfy the desired requirement.

Finally, we employ the resolvent identity to “glue” the inverse operators of the small boxes to the large box λ_N , thereby establishing the bounded inverse and the off-diagonal decay of its entries. For the central box Λ_{10K} , the resolvent identity reads

$$|T_N^{-1}(\mathbf{k}_1, \mathbf{k}_2)| \leq |T_{\Lambda_{10K}}^{-1}(\mathbf{k}_1, \mathbf{k}_2)| + \sum_{\mathbf{k}_3 \in \Lambda_{10K}} \sum_{\mathbf{k}_4 \in \Lambda_N \setminus \Lambda_{10K}} |T_{\Lambda_{10K}}^{-1}(\mathbf{k}_1, \mathbf{k}_3)| |T(\mathbf{k}_3, \mathbf{k}_4)| |T_{\Lambda_{10K}}^{-1}(\mathbf{k}_4, \mathbf{k}_2)|, \quad (6.5)$$

where $\mathbf{k}_4 \in \Lambda_N / \Lambda_{10K}$. Although $|T_{\Lambda_{10K}}^{-1}(\mathbf{k}_1, \mathbf{k}_3)|$ must satisfy the two-side off-diagonal decay, $T(\mathbf{k}_3, \mathbf{k}_4)$ satisfies the single-side off-diagonal decay as Theorem 4.7 and Theorem 5.4. For the intermediate boxes Γ_α , the resolvent identity reads

$$|T_N^{-1}(\mathbf{k}_1, \mathbf{k}_2)| \leq |T_{\Gamma_\alpha}^{-1}(\mathbf{k}_1, \mathbf{k}_2)| + \sum_{\mathbf{k}_3 \in \Gamma_\alpha} \sum_{\mathbf{k}_4 \in \Lambda_N \setminus \Gamma_\alpha} |T_{\Gamma_\alpha}^{-1}(\mathbf{k}_1, \mathbf{k}_3)| |T(\mathbf{k}_3, \mathbf{k}_4)| |T_{\Gamma_\alpha}^{-1}(\mathbf{k}_4, \mathbf{k}_2)|, \quad (6.6)$$

where $\mathbf{k}_4 \in \Lambda_{10K}$. In this case, $T_{\Gamma_\alpha}^{-1}(\mathbf{k}_3, \mathbf{k}_4)$ satisfies the single-side off-diagonal decay. The remaining steps for verifying Theorem 3.6 involve standard inequality manipulations, which are deferred to Section C.1.

6.2 The iteration lemma

Before proceeding to the inductive estimates, we must characterize the derivative of the inverse operator $\partial(T + \epsilon B)_N^{-1}$, specifically regarding its norm bounds and off-diagonal decay properties. Using the standard operator identity $(T + \epsilon B)_N^{-1}(T + \epsilon B)_N = I$, the derivative of the inverse is given by:

$$\partial(T + \epsilon B)_N^{-1} = -(T + \epsilon B)_N^{-1}(\partial(T + \epsilon B)_N)(T + \epsilon B)_N^{-1}. \quad (6.7)$$

This relationship allows us to establish the following lemma regarding the operator's composite norm and spatial localization.

Lemma 6.1. If the restricted operator $(T + \epsilon B)_N$ satisfies Theorem 3.6, then its inverse satisfies the norm bound:

$$\|\partial(T + \epsilon B)_N^{-1}\|_2 \leq \frac{4N}{\epsilon_N^2}. \quad (6.8)$$

Furthermore, for sufficiently large spatial separations in the lattice Λ_N , specifically when $|\mathbf{k} \pm \mathbf{k}'| \geq N^{\frac{3}{4}}$ the entries of the inverse matrix must exhibit Gevrey-type decay:

$$|\partial(T + \epsilon B)_N^{-1}(\mathbf{k}, \mathbf{k}')| \leq \exp\left\{-\frac{|\mathbf{k} - \mathbf{k}'|^s}{4}\right\} + \exp\left\{-\frac{|\mathbf{k} + \mathbf{k}'|^s}{4}\right\}. \quad (6.9)$$

The inversion result (6.8) follows directly from the inversion condition (3.13) and the derivative identity (6.7). The localization result (6.9) involves basic inequality derivations regarding Gevrey classes; the full technical details are deferred to Section C.2. With the verification of Theorem 3.6 and Theorem 6.1, we establish the following rigorous iteration lemma. For technical convenience, we adopt the convention that $N_{-1} = 0$ and $\Lambda_{N_{-1}} = \emptyset$.

Theorem 6.2 (The Iteration Lemma). Assume that the frequencies satisfy $\omega \in \Omega \setminus (\Omega_M^\tau \cup \Omega_1 \cup \Omega_2)$. Let $\epsilon_0 = \epsilon_0(H_1, \Omega, \mathbf{a}) > 0$ be the threshold provided in Theorem 2.2. For any $0 < \epsilon \leq \epsilon_0$, there exists a Gevrey exponent $s(\epsilon) > 0$ such that, at the r -th iteration, the approximate solution $\hat{\mathbf{z}}^{(r)}$ is supported on:

$$\text{supp } \hat{\mathbf{z}}^{(r)} \subseteq \Lambda_{N_r} = \Lambda_{M^r}. \quad (6.10)$$

Moreover, for any index $m = \{0, 1, \dots, r\}$ and any $\mathbf{k} \in \Lambda_{M^m} \setminus \Lambda_{M^{m-1}}$, assume the following Gevrey decay property holds:

$$\|\hat{\mathbf{z}}^{(r)}(\mathbf{k})\| \leq \sum_{\ell=m}^r \exp\left\{-\frac{3}{2}N_\ell^s\right\}, \quad (6.11)$$

the vector field F satisfies:

$$\|F(\hat{\mathbf{z}}_p^{(r)}; \boldsymbol{\omega}^{(r+1)}, \mathbf{a})\| \leq \exp\{-2N_r^s\}, \quad (6.12)$$

Then, after updating the frequency via Q -equations (2.19) and the coefficients via the dimension-enlarged Newton scheme (2.22), these properties are preserved at the $(r+1)$ -th iteration. Specifically, the update iterate $\hat{\mathbf{z}}^{(r+1)}$ satisfies:

$$\text{supp } \hat{\mathbf{z}}^{(r+1)} \subseteq [-N_{r+1}, N_{r+1}]^n. \quad (6.13)$$

Furthermore, for any $m \in \{0, 1, \dots, r+1\}$ and any $\mathbf{k} \in \Lambda_{M^m} \setminus \Lambda_{M^{m-1}}$, the following decay property holds:

$$\|\hat{\mathbf{z}}^{(r+1)}(\mathbf{k})\| \leq \sum_{\ell=m}^{r+1} \exp\left\{-\frac{3}{2}N_\ell^s\right\}, \quad (6.14)$$

the vector field F satisfies:

$$\|F(\hat{\mathbf{z}}_p^{(r+1)}; \boldsymbol{\omega}^{(r+2)}, \mathbf{a})\| \leq \exp\{-2N_{r+1}^s\}. \quad (6.15)$$

Proof of Theorem 6.2. For conciseness, we suppress the auxiliary parameters from the dimension-enlarged Newton scheme (2.22) and define the iterative update as:

$$\Delta^{(r)} = \hat{\mathbf{z}}_p^{(r+1)} - \hat{\mathbf{z}}_p^{(r)} = -(T + \varepsilon B)_{N_{r+1}}^{-1}(\hat{\mathbf{z}}_p^{(r)}) F(\hat{\mathbf{z}}_p^{(r)}). \quad (6.16)$$

The proof is organized in the following three steps.

Support enlargement This step verifies the inclusion property (6.13). Given the perturbation Hamiltonian H_1 is a polynomial with the total degree at most d , the vector field is located in the support as

$$\text{supp } F(\hat{\mathbf{z}}_p^{(r)}) \subseteq [-dN_r, dN_r]^n \subseteq \left[-\frac{N_{r+1}}{4}, \frac{N_{r+1}}{4}\right]^n, \quad (6.17)$$

which confirms (6.13) in accordance with the update rule defined in (6.16).

Lattice vector decay This step establishes the bound in (6.14). Given the inversion condition (3.13) and the previous vector field estimate (6.12), we bound the iterative difference as:

$$\|\Delta^{(r)}\|_2 \leq \|(T + \varepsilon B)_{N_{r+1}}^{-1}(\hat{\mathbf{z}}_p^{(r)})\|_2 \|F(\hat{\mathbf{z}}_p^{(r)})\|_2 \leq \frac{1}{\varepsilon_{N_{r+1}}} \exp\{-2N_r^s\}.$$

Furthermore, by applying Theorem 6.1, we estimate the derivative of the update. The derivative satisfies:

$$\begin{aligned} \|\partial \Delta^{(r)}\|_2 &\leq \|\partial(T + \varepsilon B)_{N_{r+1}}^{-1}(\hat{\mathbf{z}}_p^{(r)})\|_2 \|F(\hat{\mathbf{z}}_p^{(r)})\|_2 + \|(T + \varepsilon B)_{N_{r+1}}^{-1}(\hat{\mathbf{z}}_p^{(r)})\|_2 \|\partial F(\hat{\mathbf{z}}_p^{(r)})\|_2 \\ &\leq \left(\frac{4n\sqrt{N_{r+1}} + \varepsilon_{N_{r+1}}}{\varepsilon_{N_{r+1}}^2}\right) \exp\{-2N_r^s\}. \end{aligned}$$

By combining the two bounds above, we can establish a threshold $\varepsilon_0 > 0$ such that

$$\|\Delta^{(r)}\| \leq \exp\left\{-\frac{7N_r^s}{4}\right\} \quad (6.18)$$

for any $0 < \varepsilon \leq \varepsilon_0$. Now, choosing $s = s(\varepsilon) > 0$ such that $6M^s \leq 7$. Then, at the $(r+1)$ -th iteration, for any index $m = \{0, 1, \dots, r+1\}$ and any $\mathbf{k} \in \Lambda_{M^m} \setminus \Lambda_{M^{m-1}}$, the following holds:

$$\|\widehat{\mathbf{z}}^{(r+1)}(\mathbf{k})\| \leq \|\widehat{\mathbf{z}}^{(r)}(\mathbf{k})\| + \|\Delta^{(r)}(\mathbf{k})\| \leq \sum_{\ell=m}^{r+1} \exp\left\{-\frac{3}{2}N_\ell^s\right\}$$

which confirms the decay property (6.14) across successive iterations.

Super-exponential convergence To establish the super-convergence property in (6.15), we analyze the vector field after the Newton update (6.16). By applying a Taylor expansion to the vector field and the frequency, and invoking Theorem 3.4, the post-update residual can be bounded by the truncation error and the quadratic terms of the iteration:

$$\|F(\widehat{\mathbf{z}}_p^{(r+1)}; \boldsymbol{\omega}^{(r+2)})\|_2 \leq \|[(T + \varepsilon B) - (T + \varepsilon B)_{N_{r+1}}]\Delta^{(r)}\|_2 + \exp\{-3N_{r+1}^s\}, \quad (6.19)$$

while the derivative of the residual satisfies the following bound:

$$\begin{aligned} \|\partial F(\widehat{\mathbf{z}}_p^{(r+1)}; \boldsymbol{\omega}^{(r+2)})\|_2 &\leq \|\partial[(T + \varepsilon B) - (T + \varepsilon B)_{N_{r+1}}]\Delta^{(r)}\|_2 \\ &\quad + \|[(T + \varepsilon B) - (T + \varepsilon B)_{N_{r+1}}]\partial\Delta^{(r)}\|_2 + 3\exp\{-3N_{r+1}^s\}. \end{aligned} \quad (6.20)$$

To estimate the Gevery norms in (6.19) and (6.20), we exploit the off-diagonal decay of the operators $T + \varepsilon B$ and $(T + \varepsilon B)_{N_{r+1}}^{-1}$ established in Theorem 3.2 and Theorem 6.1. Since the estimation procedures for these terms are analogous, we focus on $[(T + \varepsilon B) - (T + \varepsilon B)_{N_{r+1}}]\Delta^{(r)}$ as the representative example. We utilize the following decomposition:

$$\begin{aligned} [(T + \varepsilon B) - (T + \varepsilon B)_{N_{r+1}}]\Delta^{(r)} &= [(I - P_{N_{r+1}})(T + \varepsilon B)P_{N_{r+1}}] \left[(I - P_{N_{r+1}/3})\Delta^{(r)} \right] \\ &\quad + [(I - P_{N_{r+1}})(T + \varepsilon B)P_{N_{r+1}/3}] \Delta^{(r)}. \end{aligned} \quad (6.21)$$

Given the confirmed off-diagonal decay, there exists a threshold $\varepsilon_0 > 0$ such that for $0 < \varepsilon \leq \varepsilon_0$, the following estimates holds:

$$\|(I - P_{N_{r+1}})(T + \varepsilon B)P_{N_{r+1}/3}\| \leq \frac{1}{3} \exp\left\{-\frac{7}{12}N_{r+1}^s\right\} \quad (6.22)$$

and

$$\|(I - P_{N_{r+1}/3})(T + \varepsilon B)_{N_{r+1}}^{-1}P_{N_{r+1}/4}\| \leq \frac{1}{3} \exp\left\{-\frac{1}{48}N_{r+1}^s\right\} \quad (6.23)$$

Noting that $\|(I - P_{N_{r+1}})TP_{N_{r+1}}\| \leq \|S\| \leq 1$, we combine the bounds (6.22) and (6.23) with the decomposition in (6.21) to account for the truncation error from (6.19) and (6.20). For a suitably chosen threshold $\varepsilon_0 > 0$, we obtain

$$\|F(\widehat{\mathbf{z}}_p^{(r+1)}; \boldsymbol{\omega}^{(r+2)})\| \leq \frac{2}{3} \exp\left\{-\left(\frac{2}{M^s} + \frac{1}{48}\right)N_{r+1}^s\right\} + 4\exp\{-3N_{r+1}^s\} \quad (6.24)$$

By choosing $s = s(\varepsilon) > 0$ such that $95M^s \leq 96$, we arrive at the desired super-convergence bound:

$$\|F(\hat{\mathbf{z}}_p^{(r+1)}; \boldsymbol{\omega}^{(r+2)})\|_s \leq \exp\{-2N_{r+1}^s\}, \quad (6.25)$$

which concludes the proof of the Iteration Lemma (Theorem 6.2). \square

Remark 6.3. Regarding the decay estimates for lattice vectors specified in (6.11) and (6.14) of Lemma 6.2: while the individual estimates might appear to grow intermittently upon initial inspection, the cumulative decay remains well-controlled. Specifically, for any multi-index $\mathbf{k} \in \Lambda_{N_r} \setminus \Lambda_{N_{r-1}}$, the following holds:

$$\sum_{\ell=r}^{\infty} \exp\left\{-\frac{3N_{\ell}^s}{2}\right\} \leq \exp\{-N_r^s\} \leq \exp\{-|\mathbf{k}|^s\},$$

which demonstrates that at each iteration r , the sequence $\hat{\mathbf{z}}^{(r)}$ remains within the space $\mathcal{K}(s)$. Consequently, the solution preserves the s -Gevrey decay property throughout the iterative process, ensuring that the spatial localization does not degrade as the lattice size N increases.

Proof of Theorem 2.2 First, we observe that (6.18) holds when $\hat{\mathbf{z}}_p$ is replaced by $\hat{\mathbf{z}}$ as $\hat{\mathbf{z}}_q^{(r)}$ remains constant at each step. The displacement between successive iterations is bounded as:

$$\|\hat{\mathbf{z}}^{(r+1)} - \hat{\mathbf{z}}^{(r)}\| = \|\Delta^{(r)}\| \leq \exp\left\{-\frac{7}{4}N_r^s\right\} = \exp\left\{-\frac{7}{4}(M^s)^r\right\}.$$

This implies the convergence of the sequences $\{\hat{\mathbf{z}}^{(r)}\}$. Furthermore, we can bound the distance to the limit \mathbf{z}^* by estimating the tail of the sequence:

$$\begin{aligned} \|\hat{\mathbf{z}}^{(r)} - \hat{\mathbf{z}}^*\| &\leq \sum_{l=0}^{\infty} \|\hat{\mathbf{z}}^{(r+l+1)} - \hat{\mathbf{z}}^{(r+l)}\| \leq \sum_{l=0}^{\infty} \exp\left\{-\frac{7}{4}(M^s)^{r+l}\right\} \\ &\leq \exp\left\{-\frac{3}{2}(M^s)^r\right\}, \end{aligned}$$

which confirms (2.25a). Moreover, from Q -equations (2.19) and the uniform bound (3.6), we have:

$$|\boldsymbol{\omega}^{(r+1)} - \boldsymbol{\omega}^{(r)}| \leq \varepsilon\gamma \|\hat{\mathbf{z}}^{(r+1)} - \hat{\mathbf{z}}^{(r)}\| \leq \varepsilon\gamma \exp\left\{-\frac{7}{4}(M^s)^r\right\}.$$

Thus, the convergence of the frequency sequences $\{\boldsymbol{\omega}^{(r)}\}$ follows, and we also have

$$\begin{aligned} |\boldsymbol{\omega}^{(r)} - \boldsymbol{\omega}^*| &\leq \sum_{l=0}^{\infty} |\boldsymbol{\omega}^{(r+l+1)} - \boldsymbol{\omega}^{(r+l)}| \leq \sum_{l=0}^{\infty} \varepsilon\gamma \exp\left\{-\frac{7}{4}(M^s)^{r+l}\right\} \\ &\leq \exp\left\{-\frac{3}{2}(M^s)^r\right\}, \end{aligned}$$

which confirms (2.25b).

Finally, we write the exact solution in a Fourier expansion

$$z^*(t) = \sum_{\mathbf{k} \in \mathbb{Z}^n} \widehat{z}^*(\mathbf{k}) e^{i\langle \omega^*, \mathbf{k} \rangle t},$$

From the support property (6.10), the error can be split into two terms:

$$\begin{aligned} \|\mathbf{z}^{(r)}(t) - \mathbf{z}^*(t)\| &\leq \left\| \sum_{\mathbf{k} \in \mathbb{Z}^n} (\widehat{z}^*(\mathbf{k}) - \widehat{z}^{(r)}(\mathbf{k})) e^{i\langle \omega^*, \mathbf{k} \rangle t} \right\| + \left\| \sum_{\mathbf{k} \in \Lambda_{M^{r+1}}} \widehat{z}^{(r)}(\mathbf{k}) (e^{i\langle \omega^*, \mathbf{k} \rangle t} - e^{i\langle \omega^{(r)}, \mathbf{k} \rangle t}) \right\| \\ &\triangleq I_1 + I_2. \end{aligned}$$

By (6.10), Gevrey decay property (6.11), the Cauchy-Schwarz inequality, and (2.25a) just proved above, we estimate the term I_1 as

$$\begin{aligned} I_1 &\leq \sum_{\mathbf{k} \in \Lambda_{M^{r+1}}} \|\widehat{z}^*(\mathbf{k}) - \widehat{z}^{(r)}(\mathbf{k})\| + \sum_{\mathbf{k} \notin \Lambda_{M^{r+1}}} \|\widehat{z}^*(\mathbf{k})\| \\ &\leq \|\widehat{\mathbf{z}}^{(r)} - \widehat{\mathbf{z}}^*\| \cdot (2M^{r+1} + 1)^{n/2} + \sum_{\mathbf{k} \notin \Lambda_{M^{r+1}}} e^{-\frac{5}{4}|\mathbf{k}|^s} \\ &\leq \frac{1}{2} \exp \{-(M^s)^r\}. \end{aligned}$$

From the uniform boundedness of $\|\widehat{\mathbf{z}}^{(r)}\|$, a Taylor expansion of the exponential term, and the Cauchy-Schwarz inequality, we estimate the term I_2 as

$$\begin{aligned} I_2 &\leq \|\widehat{\mathbf{z}}^{(r)}\| \left(\sum_{\mathbf{k} \in \Lambda_{M^{r+1}}} (e^{i\langle \omega^*, \mathbf{k} \rangle t} - e^{i\langle \omega^{(r)}, \mathbf{k} \rangle t})^2 \right)^{\frac{1}{2}} \\ &\leq \left(\|\widehat{\mathbf{z}}^*\| + \exp \left\{ -\frac{3}{2}(M^s)^r \right\} \right) \cdot |\omega^{(r)} - \omega^*| \cdot \left(\sum_{\mathbf{k} \in \Lambda_{M^{r+1}}} \|\mathbf{k}t\|^2 \right)^{\frac{1}{2}} \\ &\leq \frac{1}{2} \exp \{-(M^s)^r\}, \end{aligned}$$

which holds for any $t \in [0, N_r] = [0, M^r]$. By combining the estimate for terms I_1 and I_2 , we obtain the final time-domain error bound (2.26), which completes the proof of Theorem 2.2.

7 Numerical Experiments

In this section, we demonstrate the computational efficiency of the proposed alternating numerical procedure (see Figure 4). The key feature of this iterative scheme lies in its decoupled refinement strategy: the Q -equations (2.12) are employed to update the frequency via the iterative scheme (2.19), while the dimension-enlarged Newton scheme (2.22) is implemented to solve the P -equations (2.14) and derive the non-resonant vectors. To demonstrate the versatility and robustness of the method, we apply it to two classical benchmark problems in nonlinear dynamics: the undamped Duffing oscillator and the Hénon-Heiles model.

7.1 Undamped Duffing oscillator

The undamped Duffing oscillator serves as a classical model for Hamilton systems featuring cubic nonlinearities; see, for instance, [Kanamaru \[2008\]](#). The Hamiltonian $H = H(x, y)$, defined on the phase space $(x, y) \in \mathbb{R}^2$, takes the form

$$H = H(x, y) = \frac{1}{2}(x^2 + y^2) + \frac{\varepsilon}{4}y^4, \quad (7.1)$$

where the system is equipped with the standard symplectic two-form $\omega = dx \wedge dy$. To facilitate the application of our alternating numerical procedure, we introduce the complex coordinates:

$$\begin{cases} z = \frac{1}{\sqrt{2}}(y - ix), \end{cases} \quad (7.2a)$$

$$\begin{cases} \bar{z} = \frac{1}{\sqrt{2}}(y + ix) \end{cases} \quad (7.2b)$$

Substituting the coordinate transformation (7.2) into the Hamiltonian (7.1), the Hamiltonian $H = H(z, \bar{z})$ can be rewritten in complex form as

$$H = H(z, \bar{z}) = |z|^2 + \frac{\varepsilon}{16}(z + \bar{z})^4, \quad (7.3)$$

with the symplectic structures preserved as $dz \wedge d\bar{z} = -idx \wedge dy$. Earlier mathematical studies of this model have focused on quasi-periodic solutions through the lens of the Poincaré map and the Moser twist theorem. These approaches establish the existence of invariant tori and Lagrange stability (e.g., [Yuan \[1998, 2000\]](#)), which ensure the long-term boundedness of the system's trajectories.

We demonstrate the efficiency of our alternating numerical procedure using a perturbation parameter of $\varepsilon = 1$. The evolution of the phase trajectories for iterations $r = 1$ to $r = 5$ is illustrated in Figure 8. Starting from the linear solution serving as the initial approximation, the method rapidly captures the nonlinear dynamics. By the second iteration, the solution at $t = 10$ already reaches a position significantly close to the accurate trajectory. At the third iteration, the trajectory becomes almost indistinguishable from the exact solution, with an error on the scale $O(0.01)$. For $r = 4$ and $r = 5$, the results become so refined that they are practically indistinguishable, even under a magnified zoom-in view. To further assess the accuracy of the method, we examine the iteration errors, which exhibit super-exponential convergence, as illustrated in Figure 9. Specifically, we track the following quantities: (i) the Fourier coefficient error, $\|\hat{\mathbf{z}}^{(r+1)} - \hat{\mathbf{z}}^{(r+1)}\|$, measuring the convergence of the coefficients, (ii) the frequency error, $|\boldsymbol{\omega}^{r+1} - \boldsymbol{\omega}^r|$, quantifying the refinement of the computed frequency, and (iii) the pointwise solution error at $t = 10$, $|\mathbf{z}^{(r+1)}(10) - \mathbf{z}^{(r)}(10)|$, evaluating the discrepancy of the solution at a fixed time. All three metrics consistently confirm the rapid convergence behavior of the proposed alternating scheme.

7.2 The Hénon-Heiles model

While a one-dimensional Duffing system is sufficient to demonstrate the basic efficiency of our alternating numerical procedure, it is inherently limited. To fully capture the complexity of quasi-periodic solutions and the structural evolution of phase space, a higher-dimensional system is required. We therefore consider the Hénon-Heiles model, a two-dimensional cornerstone of celestial

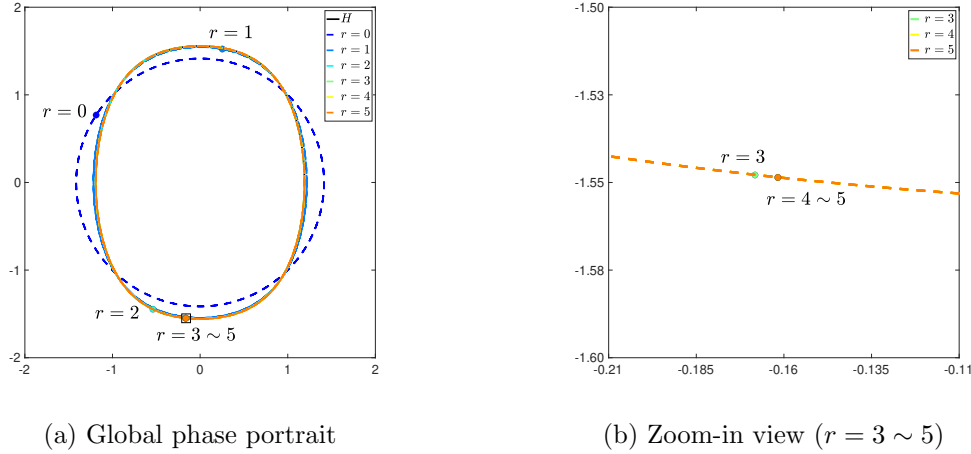


Figure 8: Phase space trajectories of the Duffing oscillator with states labeled at $t = 10$. The global view (a) illustrates the overall flows, while the magnification (b) highlights the rapid convergence toward the target state at $t = 10$.

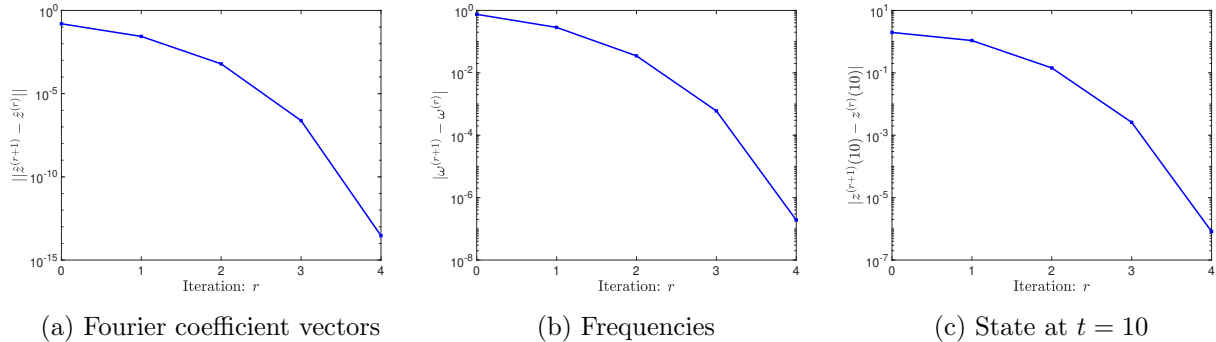


Figure 9: Convergence profiles across iterations for the Duffing system. The plots demonstrate the super-exponential decay of residuals for (a) the Fourier coefficient vector, (b) the identified frequencies, and (c) the solution state at $t = 10$.

mechanics originally developed to describe stellar motion within an axisymmetric galactic potential [Hénon and Heiles, 1964]. The Hamiltonian $H = H(x_1, x_2; y_1, y_2)$, defined on \mathbb{R}^4 , takes the form

$$H = H(x_1, x_2, y_1, y_2) = \frac{1}{2}\omega_1(x_1^2 + y_1^2) + \frac{1}{2}\omega_2(x_2^2 + y_2^2) + \varepsilon(y_1^2 y_2 - \frac{1}{3}y_2^3), \quad (7.4)$$

with the symplectic two-form $\omega = dx_1 \wedge dy_1 + dx_2 \wedge dy_2$. Similarly, to implement our alternating numerical procedure, we apply the complex coordinate transformation (7.2) into the Hamiltonian (7.4) as

$$H = H(z, \bar{z}) = \omega_1|z_1|^2 + \omega_2|z_2|^2 + \varepsilon \left[\frac{1}{2\sqrt{2}}(z_1 + \bar{z}_1)^2(z_2 + \bar{z}_2) - \frac{1}{6\sqrt{2}}(z_2 + \bar{z}_2)^3 \right], \quad (7.5)$$

where the symplectic form is expressed as $w = dz_1 \wedge d\bar{z}_1 + dz_2 \wedge d\bar{z}_2 = -i(dx_1 \wedge dy_1 + dx_2 \wedge dy_2)$. As a nearly-integrable system, this model serves as a rigorous testing ground for both perturbation theory and numerical integration. It comprises a harmonic oscillator base coupled with third-order

nonlinear terms that trigger a transition from ordered to chaotic motion as energy increases. The mathematical complexity of its nearly-integrable coupling was further formalized by [Channell and Scovel \[1990\]](#), who utilized the model to demonstrate how symplectic integrators maintain the structural integrity of the phase space over long temporal scales.

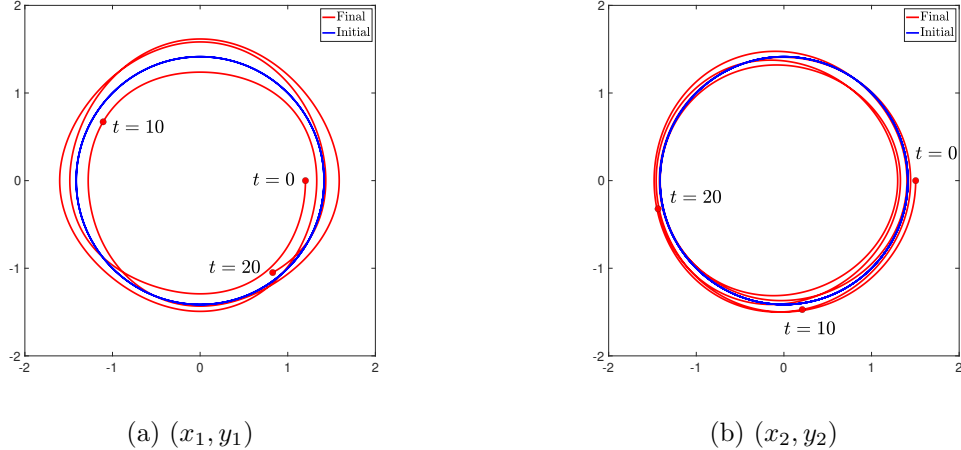


Figure 10: Phase space trajectories of the Hénon–Heiles model. The evolution of system states is highlighted at discrete time intervals ($t = 0$, $t = 10$, and $t = 20$), illustrating the dynamic progression of the trajectory.

While symplectic methods are renowned for preserving the “shape” of the orbit, specifically the invariant tori, they often suffer from the accumulation of phase-lag errors over long integration periods. As a result, even when the qualitative shape of the orbit is maintained, the numerical trajectory may gradually drift along the torus. Our alternating numerical procedure effectively addresses this limitation by precisely predicting the instantaneous positions and phase angles along these trajectories. With the perturbation parameter set to $\varepsilon = 0.1$, Figure 10 demonstrates that our method captures the exact state of the system within the two phase planes (x_1, y_1) and (x_2, y_2) . From a theoretical sense, independently of computational resource constraints, the proposed procedure allows phase-lag errors to be reduced arbitrarily. Consequently, the particle’s position at any prescribed time can be computed with high precision, thereby eliminating the temporal drift that typically compromises the long-term reliability of conventional Hamiltonian simulations. Furthermore, we exhibit super-exponential convergence in Figure 12 for both the Fourier coefficient error, $\|\widehat{\mathbf{z}}^{(r+1)} - \widehat{\mathbf{z}}^{(r+1)}\|$ and the pointwise solution error at $t = 10$, $|\mathbf{z}^{(r+1)}(10) - \mathbf{z}^{(r)}(10)|$. A subtle point requires attention here: the support for the complex Hamilton vector field $\mathbf{X} = (\partial H / \partial \bar{z}_1, \partial H / \partial z_2)$ does not include \mathbf{e}_1 and \mathbf{e}_2 as given by:

$$\begin{cases} \text{supp} \widehat{\frac{\partial H}{\partial \bar{z}_1}} = \{\pm \mathbf{e}_1 \pm \mathbf{e}_2\} \\ \text{supp} \widehat{\frac{\partial H}{\partial z_2}} = \{0, \pm 2\mathbf{e}_1, \pm 2\mathbf{e}_2\} \end{cases}$$

Thus, the vector field associated with the Q -equations in (2.12) is zero, meaning that the associated frequency update (2.19) remains invariant during the first step. The resulting numerical perfor-

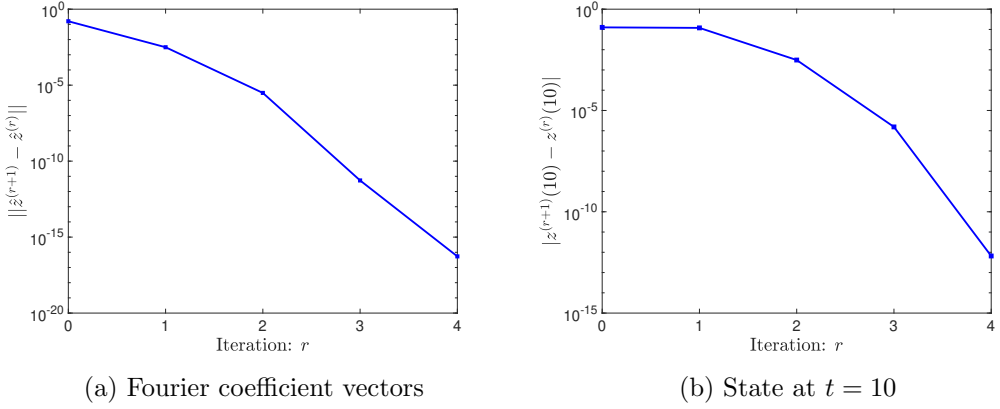


Figure 11: Convergence profiles across iterations for the Hénon–Heiles model. (a) Norm decay of the Fourier coefficient vector. (b) Numerical solution state evaluated at $t = 10$.

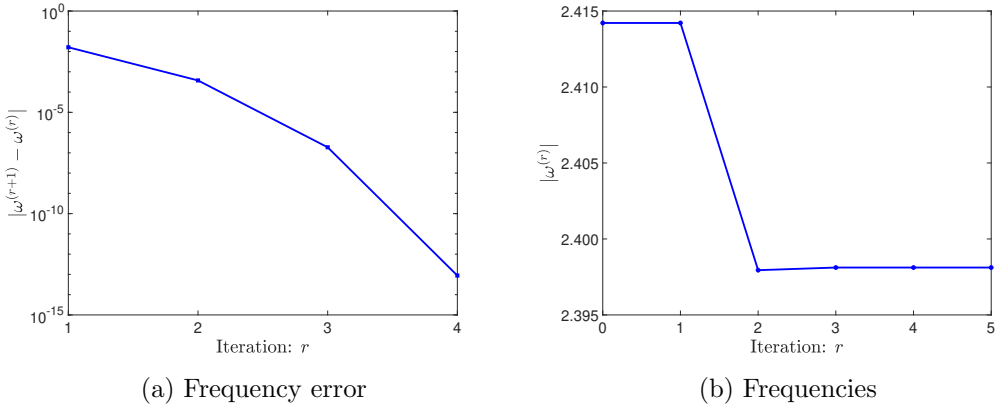


Figure 12: The behavior of frequencies across iterations for the Hénon–Heiles model. (a) Reduction of frequency error. (b) The frequency iteration.

mance for the frequency iteration, which clearly illustrates this super-exponential convergence, is depicted in Figure 12.

8 Conclusion and further work

In this study, we developed an alternating numerical procedure that bridges the gap between theoretical infinite-dimensional analysis and practical computation. By introducing a numerical update for frequency derived from the Q-equations, we successfully integrated an iterative framework with the dimension-enlarged Newton scheme (Nash-Moser scheme) for P-equations. This work establishes a novel computational pathway for the CWB framework, enabling the practical application of previously abstract theoretical constructs. The scheme achieves arbitrary numerical accuracy in capturing the intricate dynamics of quasi-periodic solutions within nearly-integrable Hamiltonian systems, providing a functional realization of the CWB scheme. We have significantly streamlined the multi-scale analysis developed by Bourgain [1998] to establish the convergence of this

algorithm. This simplification ensures that the numerical results maintain rigorous mathematical integrity while remaining computationally accessible.

The methodology presented here lays the groundwork for several extensions. Our immediate focus involves the computation of lower-dimensional quasi-periodic solutions for finite-dimensional systems. In forthcoming work, we will investigate the numerical acquisition of quasi-periodic solutions for nonlinear partial differential equations (PDEs) using this alternating algorithm. Further research will examine numerical convergence and stability, specifically focusing on the influence of small divisors on the robustness and efficiency of the expanded numerical scheme.

Acknowledgements

This work was partially supported by the NSFC (Grant No. 12241105) and by SIMIS (startup fund and cross-disciplinary research projects).

References

- V. I. Arnold. Small divisor problems in classical and celestial mechanics. *Russian Mathematical Surveys*, 18(6):85–191, 1963.
- V. I. Arnol'd. *Mathematical methods of classical mechanics*, volume 60. Springer Science & Business Media, 2013.
- V. I. Arnold, V. V. Kozlov, and A. I. Neishtadt. *Mathematical Aspects of Classical and Celestial Mechanics*, volume 3 of *Encyclopaedia of Mathematical Sciences*. Springer Berlin, Heidelberg, 3 edition, 2006.
- J. Bourgain. Construction of quasi-periodic solutions for Hamiltonian perturbations of linear equations and applications to nonlinear PDE. *International Mathematics Research Notices*, 1994(11):475–497, 1994.
- J. Bourgain. Quasi-periodic solutions of Hamiltonian perturbations of 2D linear Schrödinger equations. *Annals of Mathematics*, pages 363–439, 1998.
- J. Bourgain. *Green's Function Estimates for Lattice Schrödinger Operators and Applications*. Princeton University Press, Princeton, 2005.
- P. J. Channell and C. Scovel. Symplectic integration of Hamiltonian systems. *Nonlinearity*, 3(2):231, 1990.
- D. Cohen, E. Hairer, and C. Lubich. Modulated Fourier expansions of highly oscillatory differential equations. *Foundations of Computational Mathematics*, 3(4):327–345, 2003.
- W. Craig and C. E. Wayne. Newton's method and periodic solutions of nonlinear wave equations. *Communications on Pure and Applied Mathematics*, 46(11):1409–1498, 1993.
- R. De Vogelaere. Methods of integration which preserve the contact transformation property of the Hamiltonian equations. Technical Report 4, Department of Mathematics, University of Notre Dame, Notre Dame, IN, 1956.

K. Feng. On difference schemes and symplectic geometry. In *Proceedings of the Fifth International Symposium on Differential Geometry and Differential Equations, August 1984, Beijing*, pages 42–58, Beijing, 1985.

K. Feng. Difference schemes for Hamiltonian formalism and symplectic geometry. *Journal of Computational Mathematics*, 4:279–289, 1986.

K. Feng. Formal power series and numerical algorithms for dynamical systems. In T. Chan and Z.-C. Shi, editors, *Proceedings of the International Conference on Scientific Computation*, volume 1 of *Series on Applied Mathematics*, pages 28–35, Hangzhou, China, 1991.

K. Feng and Z. Shang. Volume-preserving algorithms for source-free dynamical systems. *Numerische Mathematik*, 71(4):451–463, 1995.

L. Gauckler, E. Hairer, and C. Lubich. Dynamics, numerical analysis, and some geometry. In *Proceedings of the International Congress of Mathematicians: Rio de Janeiro 2018*, pages 453–485. World Scientific, 2018.

G. H. Golub and C. F. Van Loan. *Matrix Computations*. JHU Press, 4 edition, 2013.

E. Hairer and C. Lubich. The life-span of backward error analysis for numerical integrators. *Numerische Mathematik*, 76(4):441–462, 1997.

E. Hairer and C. Lubich. Long-time energy conservation of numerical methods for oscillatory differential equations. *SIAM journal on numerical analysis*, 38(2):414–441, 2000.

E. Hairer and G. Wanner. *Solving Ordinary Differential Equations II: Stiff and Differential-Algebraic Problems*, volume 14 of *Springer Series in Computational Mathematics*. Springer, Berlin, Heidelberg, 2 edition, 1996.

E. Hairer, C. Lubich, and G. Wanner. Geometric numerical integration illustrated by the Störmer–Verlet method. *Acta numerica*, 12:399–450, 2003.

M. Hénon and C. Heiles. The applicability of the third integral of motion: some numerical experiments. *Astronomical Journal*, 69:73–79, 1964.

M. I. Jordan. Dynamical, symplectic and stochastic perspectives on gradient-based optimization. In *Proceedings of the international congress of mathematicians: Rio de Janeiro 2018*, pages 523–549. World Scientific, 2018.

T. Kanamaru. Duffing oscillator. *Scholarpedia*, 3(3):6327, 2008.

S. B. Kuksin. *Analysis of Hamiltonian PDEs*, volume 19. Clarendon Press, 2000.

B. Y. Levin. *Lectures on entire functions*, volume 150. American Mathematical Society, 1996.

J. Liu and X. Yuan. A KAM theorem for hamiltonian partial differential equations with unbounded perturbations. *Communications in mathematical physics*, 307(3):629–673, 2011.

J. Moser. A rapidly convergent iteration method and non-linear partial differential equations. I. *Annali della Scuola Normale Superiore di Pisa. Classe di Scienze*, 20(3):265–315, 1966a.

J. Moser. A rapidly convergent iteration method and non-linear partial differential equations. II. *Annali della Scuola Normale Superiore di Pisa. Classe di Scienze*, 20(3):499–535, 1966b.

J. K. Moser. On invariant curves of area-preserving mapping of an annulus. *Matematika*, 6(5):51–68, 1962.

J. Nash. The imbedding problem for Riemannian manifolds. *Annals of mathematics*, 63(1):20–63, 1956.

R. D. Ruth. A canonical integration technique. *IEEE Transactions on Nuclear Science*, NS-30:2669–2671, 1983.

Z.-J. Shang. KAM theorem of symplectic algorithms for Hamiltonian systems. *Numerische Mathematik*, 83(3):477–496, 1999.

Z.-J. Shang. Resonant and Diophantine step sizes in computing invariant tori of Hamiltonian systems. *Nonlinearity*, 13(1):299, 2000.

T. Witelski and M. Bowen. Singular perturbation theory. *Scholarpedia*, 4(4):3951, 2009.

H. Yoshida. Recent progress in the theory and application of symplectic integrators. *Celestial Mechanics and Dynamical Astronomy*, 56:27–43, 1993.

X. Yuan. Invariant tori of Duffing-type equations. *Journal of Differential Equations*, 142(2):231–262, 1998.

X. Yuan. Lagrange stability for Duffing-type equations. *Journal of Differential Equations*, 160(1):94–117, 2000.

X. Yuan. KAM theorem with normal frequencies of finite limit-points for some shallow water equations. *Communications on Pure and Applied Mathematics*, 74(6):1193–1281, 2021.

A Proofs of results in Section 3

In this appendix, we provide the detailed proofs for the results presented in Section 3, specifically addressing Theorem 3.1 (Section A.2), Theorem 3.2 (Section A.3), Theorem 3.3 (Section A.4), and Theorem 3.4 (Section A.5). To facilitate these proofs, we first establish an elementary inequality and demonstrate that the Gevrey decay property is preserved under convolution. These preliminary results are rigorously stated in the following lemmas.

A.1 Preliminary lemmas

Lemma A.1. Let $a, b \geq 0$ and $0 < s < 1$. Then the following inequality holds:

$$a^s + b^s - (a + b)^s \geq (2 - 2^s) \min\{a, b\}^s \quad (\text{A.1})$$

Proof. Assume without loss of generality that $a \geq b$. If $b = 0$, the inequality is trivial. For $b > 0$, we divide both sides of (A.1) by b^s to obtain:

$$\left(\frac{a}{b}\right)^s + 1 - \left(1 + \frac{a}{b}\right)^s \geq 2 - 2^s$$

Let $x = a/b \in [1, \infty)$ and define the function $f(x) = x^s + 1 - (1+x)^s$. Its derivative is

$$f'(x) = s \left[\frac{1}{x^{1-s}} - \frac{1}{(1+x)^{1-s}} \right].$$

Since $1-s > 0$ and $x < 1+x$, it follows that $x^{1-s} < (1+x)^{1-s}$, which implies $f'(x) > 0$. Therefore, f is monotonically increasing on $[1, \infty)$, and its minimum occurs at $x = 1$, where $f(1) = 2 - 2^s$. This completes the proof. \square

Next, we use Theorem A.1 to show that the Gevrey decay property is preserved under convolution.

Lemma A.2. Let the Gevrey decay set $\mathcal{K}(s)$ be defined in (2.24). For any two Fourier vectors $\widehat{a}, \widehat{b} \in \mathcal{K}(s)$, there exists a constant $C_2(n, s) > 0$ such that their convolution satisfies

$$\sup_{\mathbf{k} \in \mathbb{Z}^n} \left(|(\widehat{a} * \widehat{b})(\mathbf{k})| \exp \{|\mathbf{k}|^s\} \right) \leq C_2(n, s) \quad (\text{A.2})$$

More generally, if $\widehat{a}_j(\mathbf{k}) \in \mathcal{K}(s)$ for $j = 1, \dots, m$, then there exists a constant $C_m(n, s) > 0$ such that the m -fold convolution satisfies:

$$\sup_{\mathbf{k} \in \mathbb{Z}^n} \left(|(\widehat{a}_1 * \widehat{a}_2 * \dots * \widehat{a}_m)(\mathbf{k})| \exp \{|\mathbf{k}|^s\} \right) \leq C_m(n, s) \quad (\text{A.3})$$

Proof. Given that the Fourier vectors $\widehat{a}, \widehat{b} \in \mathcal{K}(s)$, we calculate their convolution as

$$\begin{aligned} |(\widehat{a} * \widehat{b})(\mathbf{k})| &\leq \sum_{\mathbf{k}' \in \mathbb{Z}^n} |\widehat{a}(\mathbf{k} - \mathbf{k}')| |\widehat{b}(\mathbf{k}')| \\ &\leq \sum_{\mathbf{k}' \in \mathbb{Z}^n} \exp \{-|\mathbf{k} - \mathbf{k}'|^s\} \exp \{-|\mathbf{k}'|^s\} \\ &\leq \sum_{\mathbf{k}' \in \mathbb{Z}^n} \exp \{-|\mathbf{k}|^s\} \exp \{-(|\mathbf{k} - \mathbf{k}'|^s + |\mathbf{k}'|^s - (|\mathbf{k} - \mathbf{k}'| + |\mathbf{k}'|)^s)\}, \end{aligned}$$

where the last step uses the triangle inequality. Applying Theorem A.1 to bound the sum involving the remaining exponential terms, we have

$$|(\widehat{a} * \widehat{b})(\mathbf{k})| \leq \exp \{-|\mathbf{k}|^s\} \left(\sum_{\mathbf{k}' \in \mathbb{Z}^n} \exp \{-(2 - 2^s) \min \{|\mathbf{k} - \mathbf{k}'|^s, |\mathbf{k}'|^s\}\} \right).$$

Since the sum of the Gevrey decay series converges in an n -dimensional lattice \mathbb{Z}^n , we establish the inequality (A.2). By induction, this same argument extends to any finite m -fold convolutional products, thereby establishing the inequalities (A.3). \square

A.2 Proof of Theorem 3.1

Since the perturbation Hamiltonian H_1 is a real-coefficient polynomial, each components of its associated vector field, $\partial H / \partial \bar{z}_j$ for $j = 1, \dots, n$, is likewise a real-coefficient polynomial. Given that $\hat{\mathbf{z}} \in \mathcal{K}(s)$, Theorem A.2 implies that the coefficient $\hat{\mathbf{X}}(\mathbf{k})$ exhibit Gevrey decay. By applying the Leibniz rule, it follows that the derivatives $\partial_{\omega} \hat{\mathbf{X}}(\mathbf{k})$ also exhibits Gevrey decay, which leads directly to the estimate in (3.2). By summing these decaying terms (leveraging the convergence of the Gevrey series) or applying the supremum bound across the domain, it follows that the total vector field is bounded. This establishes the uniform bound in (3.3).

A.3 Proof of Theorem 3.2

Following a similar argument as used for the vector field, we apply Theorem A.2 to establish Gevrey decay for the entries of the Hessian operator and their derivative with respect to the frequency ω . Since the two operators \mathcal{H}_1 and \mathcal{H}_2 exhibit Toeplitz-like and Hankel-like structures respectively, we can establish the necessary bound over the full lattice \mathbb{Z}^n . This results naturally extends to the non-resonant set in (3.5). To bound the norm for the operator \mathcal{H}_1 , we consider the norm $\mathcal{H}_1 \hat{\mathbf{z}}$ for any $\hat{\mathbf{z}} \in \ell_2$ as

$$\begin{aligned} \|\mathcal{H}_1 \hat{\mathbf{z}}\|^2 &= \sum_{\mathbf{k} \in \mathbb{Z}^n} \left\| \sum_{\mathbf{k}' \in \mathbb{Z}^n} \mathcal{H}_1(\mathbf{k}') \hat{\mathbf{z}}(\mathbf{k} - \mathbf{k}') \right\|^2 \\ &\leq \sum_{\mathbf{k} \in \mathbb{Z}^n} \left(\sum_{\mathbf{k}' \in \mathbb{Z}^n} \|\mathcal{H}_1(\mathbf{k}')\|^{\frac{1}{2}} \cdot \|\mathcal{H}_1(\mathbf{k}')\|^{\frac{1}{2}} \|\hat{\mathbf{z}}(\mathbf{k} - \mathbf{k}')\| \right)^2 \end{aligned}$$

Since the operator \mathcal{H}_1 exhibits Gevrey decay, we apply the Cauchy-Schwarz inequality to derive the following bound as

$$\|\mathcal{H}_1 \hat{\mathbf{z}}\|^2 \leq \left[\sum_{\mathbf{k} \in \mathbb{Z}^n} \|\mathcal{H}_1(\mathbf{k})\| \right]^2 \left[\sum_{\mathbf{k} \in \mathbb{Z}^n} \|\hat{\mathbf{z}}(\mathbf{k})\|^2 \right] < \infty. \quad (\text{A.4})$$

Similarly, we can establish a corresponding bound for the operator \mathcal{H}_2 as

$$\|\mathcal{H}_2 \hat{\mathbf{z}}\|^2 \leq \left[\sum_{\mathbf{k} \in \mathbb{Z}^n} \|\mathcal{H}_2(\mathbf{k})\| \right]^2 \left[\sum_{\mathbf{k} \in \mathbb{Z}^n} \|\hat{\mathbf{z}}(\mathbf{k})\|^2 \right] < \infty. \quad (\text{A.5})$$

By combining these estimates, we successfully establish the bound presented in (3.6).

A.4 Proof of Theorem 3.3

Recalling that the frequency iteration operator B from (2.21), we observe that for any $\mathbf{k}, \mathbf{k}' \in \mathcal{S}$, its entries satisfy the following inequality:

$$\|B(\mathbf{k}, \mathbf{k}')\| \leq \frac{1}{e} \left\| \frac{\partial \langle \mathbf{k}, \hat{\mathbf{X}}_q \rangle}{\partial \hat{\mathbf{z}}_p(\mathbf{k}')} \hat{\mathbf{z}}_p(\mathbf{k}) \right\|.$$

For any $\widehat{\mathbf{z}} \in \mathcal{K}(s)$, we apply the decay properties established in Theorem 3.1 to verify the Gevrey bound in (3.7). Given that B is a rank-one operator, we apply the Cauchy-Schwarz inequality to bound its norm as follows:

$$\|B(\mathbf{k}, \mathbf{k}')\| \leq \frac{1}{e} \|\mathbf{k}\widehat{\mathbf{z}}_p(\mathbf{k})\| \cdot \left\| \frac{\partial \widehat{\mathbf{X}}_q}{\partial \widehat{\mathbf{z}}_p(\mathbf{k}')} \right\|$$

By utilizing the Gevrey decay of the Hessian operators derived in Section A.3, we extend the bound over the lattice $\mathbb{Z}^n \times \mathbb{Z}^n$ as

$$\|B\| \leq \sum_{\mathbf{k} \in \mathbb{Z}^n} \left(\frac{\|\mathbf{k}\widehat{\mathbf{z}}_p(\mathbf{k})\|}{e} \right) \cdot \sum_{\mathbf{k}' \in \mathbb{Z}^n} \left(\left\| \frac{\partial \widehat{\mathbf{X}}_q}{\partial \widehat{\mathbf{z}}_p}(\mathbf{k}') \right\| \right).$$

Finally, since $\widehat{\mathbf{z}} \in \mathcal{K}(s)$, we invoke Theorem 3.1 to ensure the convergence of the infinite sum over the lattice, which confirms the uniform bound as stated in (3.8).

A.5 Proof of Theorem 3.4

As the same procedure used for vector fields and tangent linear operators, we analyze the three-order tensor $\partial^2 \widehat{\mathbf{X}} / \partial \widehat{\mathbf{z}}^2$. For any $\mathbf{k}, \mathbf{k}', \mathbf{k}'' \in \mathbb{Z}^n$, we derive the kernels as

$$\begin{aligned} \frac{\partial^2 \widehat{\mathbf{X}}(\mathbf{k})}{\partial \widehat{\mathbf{z}}(\mathbf{k}') \partial \widehat{\mathbf{z}}(\mathbf{k}'')} &= \mathcal{T}_{11}(\mathbf{k} - \mathbf{k}' - \mathbf{k}'') + \mathcal{T}_{21}(\mathbf{k} + \mathbf{k}' - \mathbf{k}'') + \mathcal{T}_{12}(\mathbf{k} - \mathbf{k}' + \mathbf{k}'') + \mathcal{T}_{22}(\mathbf{k} + \mathbf{k}' + \mathbf{k}'') \\ &= \frac{1}{(2\pi)^n} \int_{\mathbb{T}^n} \frac{\partial^3 H_1}{\partial \mathbf{z}^2 \partial \overline{\mathbf{z}}} e^{-i\langle \mathbf{k} - \mathbf{k}' - \mathbf{k}'', \boldsymbol{\theta} \rangle} d\boldsymbol{\theta} + \frac{1}{(2\pi)^n} \int_{\mathbb{T}^n} \frac{\partial^3 H_1}{\partial \mathbf{z} \partial \overline{\mathbf{z}}^2} e^{-i\langle \mathbf{k} + \mathbf{k}' - \mathbf{k}'', \boldsymbol{\theta} \rangle} d\boldsymbol{\theta} \\ &\quad + \frac{1}{(2\pi)^n} \int_{\mathbb{T}^n} \frac{\partial^3 H_1}{\partial \mathbf{z} \partial \overline{\mathbf{z}}^2} e^{-i\langle \mathbf{k} - \mathbf{k}' + \mathbf{k}'', \boldsymbol{\theta} \rangle} d\boldsymbol{\theta} + \frac{1}{(2\pi)^n} \int_{\mathbb{T}^n} \frac{\partial^3 H_1}{\partial \mathbf{z}^2 \partial \overline{\mathbf{z}}} e^{-i\langle \mathbf{k} + \mathbf{k}' + \mathbf{k}'', \boldsymbol{\theta} \rangle} d\boldsymbol{\theta}. \end{aligned}$$

Given that $\widehat{\mathbf{z}} \in \mathcal{K}(s)$ and the perturbation Hamiltonian H_1 is a real-coefficient polynomial, there exists some constant $\gamma_9 = \gamma_9(H_1, s) > 0$ such that

$$\sup_{\mathbf{k}, \mathbf{k}', \mathbf{k}'' \in \mathbb{Z}^n} \left(\|\mathcal{T}_{ij}(\mathbf{k} + (-1)^i \mathbf{k}' + (-1)^j \mathbf{k}'')\| \exp \{|\mathbf{k} + (-1)^i \mathbf{k}' + (-1)^j \mathbf{k}'''|^s\} \right) \leq \gamma_9,$$

which demonstrates that the tensors \mathcal{T}_{ij} for $i, j \in \{1, 2\}$ exhibits Gevrey decay. To establish the boundedness of the tensor, we apply the Cauchy-Schwarz inequality twice, first to decouple the \mathbf{k}'' summation and then to decouple the \mathbf{k}' convolution. Taking \mathcal{T}_{11} as a representative example, we derive the following bound:

$$\begin{aligned} \|\mathcal{T}_{11}(\widehat{\mathbf{z}}_1(\mathbf{k}'), \widehat{\mathbf{z}}_2(\mathbf{k}''))\|^2 &= \sum_{\mathbf{k} \in \mathbb{Z}^n} \left\| \sum_{\mathbf{k}'' \in \mathbb{Z}^n} \left(\sum_{\mathbf{k}' \in \mathbb{Z}^n} \mathcal{T}_{11}(\mathbf{k} - \mathbf{k}' - \mathbf{k}'') \widehat{\mathbf{z}}_1(\mathbf{k}') \right) \widehat{\mathbf{z}}_2(\mathbf{k}'') \right\|^2 \\ &\leq \left[\sum_{\mathbf{k} \in \mathbb{Z}^n} \left\| \sum_{\mathbf{k}' \in \mathbb{Z}^n} \mathcal{T}_{11}(\mathbf{k} - \mathbf{k}') \widehat{\mathbf{z}}_1(\mathbf{k}') \right\|^2 \right]^2 \left[\sum_{\mathbf{k} \in \mathbb{Z}^n} \|\widehat{\mathbf{z}}_2(\mathbf{k})\|^2 \right] \\ &\leq \left[\sum_{\mathbf{k} \in \mathbb{Z}^n} \|\mathcal{T}_{11}(\mathbf{k})\|^2 \right]^2 \left[\sum_{\mathbf{k} \in \mathbb{Z}^n} \|\widehat{\mathbf{z}}_1(\mathbf{k})\|^2 \right] \left[\sum_{\mathbf{k} \in \mathbb{Z}^n} \|\widehat{\mathbf{z}}_2(\mathbf{k})\|^2 \right] < \infty \end{aligned}$$

Similarly, we can establish the corresponding bounds for the tensors \mathcal{T}_{21} , \mathcal{T}_{12} , and \mathcal{T}_{22} . By summing these components, we establish the overall bound (3.9).

B Proofs of results in Section 4

In this appendix, we provide the detailed proofs for the results presented in Section 4, specifically addressing Theorem 4.2 and Theorem 4.4.

B.1 Proof of Theorem 4.2

Let $\Omega \in \mathbb{R}^n$ be a bounded domain, and define its diameter as $d = \max_{x,y \in \Omega} \|x - y\|_2$. For each fixed vector $\mathbf{k} \in \mathbb{Z}^n \setminus \{0\}$, the nearly-resonance condition $|\langle \mathbf{k}, \omega \rangle| < |\mathbf{k}|^{-\tau}$ defines a region in Ω bounded by two parallel hyperplanes perpendicular to \mathbf{k} . These hyperplanes enclose a “resonant strip” or slab. The distance between these hyperplanes, representing the width of the resonant strip, is at most $2\|\mathbf{k}\|_2^{-(\tau+1)}$. Therefore, we can estimate the measure of the resonant slab within the bounded domain Ω as:

$$\text{mes} \left(\left\{ \omega \in \Omega \mid |\langle \mathbf{k}, \omega \rangle| < \frac{1}{|\mathbf{k}|^\tau} \right\} \right) \leq \frac{2d^{n-1}}{\|\mathbf{k}\|_2^{\tau+1}}. \quad (\text{B.1})$$

Since the exponent satisfies $\tau > n - 1$, the lattice series $\sum_{\mathbf{k} \in \mathbb{Z}^n \setminus \{0\}} \|\mathbf{k}\|_2^{-\tau-1}$ converges. Summing the estimates in (B.1) yields the desired measure bound (4.5), which completes the proof.

B.2 Proof of Theorem 4.4

Before proceeding to the proof of Theorem 4.4, we first establish a lemma regarding the preservation of the Gevrey decay property under operator multiplication. We say that an operator $A : \ell_2(\mathbb{Z}^n) \mapsto \ell_2(\mathbb{Z}^n)$ has *proper decay* if its entries satisfy:

$$\sup_{\mathbf{k}, \mathbf{k}' \in \mathbb{Z}^n} \left(2|A(\mathbf{k}, \mathbf{k}')| (\exp \{-|\mathbf{k} - \mathbf{k}'|^s\} + \exp \{-|\mathbf{k} + \mathbf{k}'|^s\})^{-1} \right) \leq 1.$$

Lemma B.1. Let A_1 and A_2 be two operators with proper decay. Then there exists a constant $C'_2(n, s) > 0$ such that their product $\mathcal{A} = A_1 A_2$ satisfies

$$\sup_{\mathbf{k}, \mathbf{k}' \in \mathbb{Z}^n} \left(2|\mathcal{A}(\mathbf{k}, \mathbf{k}')| (\exp \{-|\mathbf{k} - \mathbf{k}'|^s\} + \exp \{-|\mathbf{k} + \mathbf{k}'|^s\})^{-1} \right) \leq C'_2(n, s) \quad (\text{B.2})$$

More generally, let A_j for $j = 1, \dots, m$ be operators with proper decay. Then there exists a constant $C'_m(n, s) > 0$ such that the m -fold product $\mathcal{A} = \prod_{j=1}^m A_j$ satisfies:

$$\sup_{\mathbf{k}, \mathbf{k}' \in \mathbb{Z}^n} \left(2|\mathcal{A}(\mathbf{k}, \mathbf{k}')| (\exp \{-|\mathbf{k} - \mathbf{k}'|^s\} + \exp \{-|\mathbf{k} + \mathbf{k}'|^s\})^{-1} \right) \leq C'_m(n, s) \quad (\text{B.3})$$

Proof. Given that A_1 and A_2 are two operators with proper decay, the entry of their product is bounded by:

$$\begin{aligned} |(\mathcal{A})(\mathbf{k}, \mathbf{k}')| &\leq \sum_{\mathbf{k}'' \in \mathbb{Z}^n} |A_1(\mathbf{k}, \mathbf{k}'')| |A_2(\mathbf{k}'', \mathbf{k}')| \\ &\leq \frac{1}{2} \sum_{\mathbf{k}'' \in \mathbb{Z}^n} (\exp \{-|\mathbf{k} - \mathbf{k}''|^s\} + \exp \{-|\mathbf{k} + \mathbf{k}''|^s\}) (\exp \{-|\mathbf{k}'' - \mathbf{k}'|^s\} + \exp \{-|\mathbf{k}'' + \mathbf{k}'|^s\}) \\ &\leq \frac{1}{2} (\exp \{-|\mathbf{k} - \mathbf{k}'|^s\} + \exp \{-|\mathbf{k} + \mathbf{k}'|^s\}) \end{aligned}$$

$$\cdot \sum_{\mathbf{k}'' \in \mathbb{Z}^n} \exp \{ -(2 - 2^s) \min \{ |\mathbf{k} \pm \mathbf{k}''|^s, |\mathbf{k}'' \pm \mathbf{k}'|^s \} \}.$$

Since the sum of the Gevrey decay series converges in an n -dimensional lattice \mathbb{Z}^n , we establish the inequality (B.2). By induction, this same argument extends to any finite m -fold products, thereby establishing the inequality (B.3). \square

We now complete the proof of Theorem 4.4. Since the diagonal operator D_N admits the uniform lower bound (4.8), it is invertible. This allows us to factor the restricted operator $(T + \varepsilon B)_N$ as follows:

$$(T + \varepsilon B)_N = D_N + \varepsilon(B_N + S_N) = D_N [I + \varepsilon D_N^{-1}(B_N + S_N)].$$

Given the smallness of the perturbation parameter ε , the operator $(T + \varepsilon B)_N$ is invertible, and its inverse can then be expanded as a Neumann series:

$$(T + \varepsilon B)_N^{-1} = [I + \varepsilon D_N^{-1}(B_N + S_N)]^{-1} D_N^{-1} = \sum_{\ell=0}^{\infty} [-\varepsilon D_N^{-1}(B_N + S_N)]^\ell D_N^{-1}. \quad (\text{B.4})$$

By applying the bound for $\|D_N^{-1}\|_2$ from (4.8) alongside the estimates from Theorem 3.2 and Theorem 3.3, we derive the following estimate as

$$\|T_N^{-1}\|_2 \leq \|D_N^{-1}\|_2 \left(\sum_{\ell=0}^{\infty} \|\varepsilon D_N^{-1}(S_N + B_N)\|_2^\ell \right) \leq \frac{1}{\varepsilon_N},$$

which establishes the norm bound (4.6). To derive the off-diagonal decay, we rewrite the Neumann series (B.4) to isolate the higher-order terms:

$$(T + \varepsilon B)_N^{-1} = D_N^{-1} - \left[\sum_{\ell=0}^{\infty} (-\varepsilon D_N^{-1}(S_N + B_N))^\ell \right] (\varepsilon D_N^{-1}(S_N + B_N) D_N^{-1}).$$

Utilizing the Gevrey decay properties for the entries of for operators S and B (Theorem 3.2 and Theorem 3.3), Theorem B.1 implies that for any $\mathbf{k} \neq \pm \mathbf{k}'$:

$$\left| (-\varepsilon D_N^{-1}(S_N + B_N))^\ell (\mathbf{k}, \mathbf{k}') \right| \leq \left(\frac{1}{2} \right)^{\ell+1} (\exp \{ -|\mathbf{k} - \mathbf{k}'|^s \} + \exp \{ -|\mathbf{k} + \mathbf{k}'|^s \}),$$

By summing the corresponding Neumann series, we establish the inequality for the off-diagonal entries (4.7). The proof of Theorem 4.4 is now complete.

B.3 Proof of Theorem 4.5

We proceed by contradiction. Suppose that the diagonal operator $D_N^{\sigma_0}$ admits two distinct diagonal entries whose absolute values are smaller than $(4n)^{-\tau}(N+1)^{-\tau}$. Specifically, for any two distinct lattice points $\mathbf{k}_1, \mathbf{k}_2 \in \mathbf{k}_0 + \Lambda_N$, assume

$$\begin{aligned} |\sigma_0 + \langle \mathbf{k}_1, \boldsymbol{\omega}' \rangle - \omega_{j_1}| &< \frac{1}{(4n)^\tau(N+1)^\tau}, \\ |\sigma_0 + \langle \mathbf{k}_2, \boldsymbol{\omega}' \rangle - \omega_{j_2}| &< \frac{1}{(4n)^\tau(N+1)^\tau}, \end{aligned}$$

for some indices $j_1, j_2, = 1, \dots, n$. According to Theorem 3.5, we apply the triangle inequality to the difference to obtain:

$$|\langle \mathbf{k}_1 - \mathbf{k}_2, \omega \rangle - \omega_{j_1} + \omega_{j_2}| < \frac{1}{(4n)^\tau (N+1)^\tau} + 2N\sqrt{\varepsilon}$$

On the other hand, since the drifted frequency vector satisfies the non-resonance condition (4.4), we have the following lower bound:

$$|\langle \mathbf{k}_1 - \mathbf{k}_2, \omega \rangle - \omega_{j_1} + \omega_{j_2}| \geq \frac{1}{|\mathbf{k}_1 - \mathbf{k}_2 - \mathbf{e}_{j_1} + \mathbf{e}_{j_2}|^\tau} \geq \frac{1}{(2n)^\tau (N+1)^\tau}$$

By choosing the threshold $\varepsilon_0 > 0$ to be sufficiently small, the upper bound derived from our assumption directly contradicts this non-resonance lower bound. This contradiction ensures that at most one such index \mathbf{k} exists, thereby completing the proof of Theorem 4.5.

C Proofs of results in Section 6

In this appendix, we provide the detailed proofs for the results presented in Section 6. Specifically, we complete the verification of Theorem 3.6 and provide the proof for Theorem 6.1.

C.1 Technical estimates for the resolvent expansion

We proceed with the verification by applying the resolvent identity to two cases defined in (6.5) and (6.6). Our objective is to establish a general bound for every entry of T_N^{-1} .

We first consider $\mathbf{k}_1 \in \Lambda_{5K}$ (and consequently, $-\mathbf{k}_1 \in \Lambda_{5K}$), as described in (6.5). The first term $|T_{\Lambda_{10K}}^{-1}(\mathbf{k}_1, \mathbf{k}_2)|$ is controlled by $\exp\{(\log 10K)^{15}\}$. To estimate the second term of in the RHS of (6.5), we note that since $\mathbf{k}_4 \notin \Lambda_{10K}$, we have $|\mathbf{k}_1 - \mathbf{k}_4| > 5K > (10K)^{\frac{1}{2}}$. By the inductive hypotheses of Theorem 3.6, we estimate $|T_{\Lambda_{10K}}^{-1}(\mathbf{k}_1, \mathbf{k}_3)|$ by using (3.14) if $|\mathbf{k}_1 \pm \mathbf{k}_3| > (10K)^{\frac{1}{2}}$ and by (3.13) otherwise. Combining these with the off-diagonal decay of $T(\mathbf{k}_3, \mathbf{k}_4)$, we arrive at the following estimate for (6.5) as

$$\begin{aligned} |T_N^{-1}(\mathbf{k}_1, \mathbf{k}_2)| &\leq \exp\{(\log 10K)^{15}\} \\ &\quad + \frac{\varepsilon}{2} \sum_{\mathbf{k}_4 \in \Lambda_N \setminus \Lambda_{10K}} \left(\exp\left\{-\frac{|\mathbf{k}_1 - \mathbf{k}_4|^s}{2}\right\} + \exp\left\{-\frac{|\mathbf{k}_1 + \mathbf{k}_4|^s}{2}\right\} \right) |T_N^{-1}(\mathbf{k}_4, \mathbf{k}_2)|. \end{aligned} \quad (\text{C.1})$$

We now consider (6.6), where $\mathbf{k}_1 \notin \Lambda_{5K}$ and the box Γ_α is centered at \mathbf{k}_1 . Here, the first term $|T_{\Gamma_\alpha}^{-1}(\mathbf{k}_1, \mathbf{k}_2)|$ is controlled by $\exp\{(\log K)^{15}\}$. Similarly, we distinguish two cases $|\mathbf{k}_1 \pm \mathbf{k}_3| > K^{\frac{1}{2}}$ and $|\mathbf{k}_1 \pm \mathbf{k}_3| \leq K^{\frac{1}{2}}$, estimating $|T_{\Gamma_\alpha}^{-1}(\mathbf{k}_1, \mathbf{k}_3)|$ via Theorem 5.4 to obtain

$$\begin{aligned} |T_N^{-1}(\mathbf{k}_1, \mathbf{k}_2)| &\leq \exp\{(\log K)^{15}\} \\ &\quad + \frac{\varepsilon}{2} \sum_{\mathbf{k}_4 \in \Lambda_N \setminus \Gamma_\alpha} \exp\left\{-\frac{|\mathbf{k}_1 - \mathbf{k}_4|^s}{2}\right\} |T_N^{-1}(\mathbf{k}_4, \mathbf{k}_2)|. \end{aligned} \quad (\text{C.2})$$

By taking the maximum of $\mathbf{k}_4 \in \Lambda_N$ for the term $|T_N^{-1}(\mathbf{k}_4, \mathbf{k}_2)|$ in both (C.1) and (C.2), we obtain:

$$\begin{aligned}
|T_N^{-1}(\mathbf{k}_1, \mathbf{k}_2)| &\leq \exp \{(\log 10K)^{15}\} \\
&\quad + \left(\max_{\mathbf{k}_4} |T_N^{-1}(\mathbf{k}_4, \mathbf{k}_2)| \right) \cdot \frac{\varepsilon}{2} \sum_{\mathbf{k}_4 \in \Lambda_N} \left(\exp \left\{ -\frac{|\mathbf{k}_1 - \mathbf{k}_4|^s}{2} \right\} + \exp \left\{ -\frac{|\mathbf{k}_1 + \mathbf{k}_4|^s}{2} \right\} \right) \\
&\leq \exp \{(\log 10K)^{15}\} + \frac{1}{2} \max_{\mathbf{k}_4} |T_N^{-1}(\mathbf{k}_4, \mathbf{k}_2)|.
\end{aligned}$$

This implies the following uniform bound:

$$|T_N^{-1}(\mathbf{k}_1, \mathbf{k}_2)| \leq 2 \exp \{(\log 10K)^{15}\}. \quad (\text{C.3})$$

To verify the off-diagonal decay (3.14), we assume $|\mathbf{k}_1 \pm \mathbf{k}_2| > N^{\frac{1}{2}} = K^5$. Since those boxes Λ_{10K} and Γ_α are of size at most $10K < K^5$, the first term in the RHS of both (6.5) and (6.6) vanish. Following the same argument above, we obtain

$$|T_N^{-1}(\mathbf{k}_1, \mathbf{k}_2)| \leq \frac{\varepsilon}{2} \sum_{\mathbf{k}_4 \in \Lambda_N \setminus \Lambda_{10K}} \left(\exp \left\{ -\frac{|\mathbf{k}_1 - \mathbf{k}_4|^s}{2} \right\} + \exp \left\{ -\frac{|\mathbf{k}_1 + \mathbf{k}_4|^s}{2} \right\} \right) |T_N^{-1}(\mathbf{k}_4, \mathbf{k}_2)|. \quad (\text{C.4})$$

and

$$|T_N^{-1}(\mathbf{k}_1, \mathbf{k}_2)| \leq \frac{\varepsilon}{2} \sum_{\mathbf{k}_4 \in \Lambda_N \setminus \Gamma_\alpha} \exp \left\{ -\frac{|\mathbf{k}_1 - \mathbf{k}_4|^s}{2} \right\} |T_N^{-1}(\mathbf{k}_4, \mathbf{k}_2)|. \quad (\text{C.5})$$

Repeated application of the iterations (C.4) and (C.5) yields the localization bound:

$$|(T + \varepsilon B)_N^{-1}(\mathbf{k}_1, \mathbf{k}_2)| \leq \exp \left\{ -\frac{|\mathbf{k}_1 - \mathbf{k}_2|^s}{2} \right\} + \exp \left\{ -\frac{|\mathbf{k}_1 + \mathbf{k}_2|^s}{2} \right\}, \quad \text{for } |\mathbf{k}_1 \pm \mathbf{k}_2| \geq N^{\frac{1}{2}}, \quad (\text{C.6})$$

which confirms (3.14).

Finally, using (C.3) and (C.6), we calculate the l_1 - and l_∞ -norm of T_N^{-1} to bound the l_2 -norm of T_N^{-1} as

$$\|T_N^{-1}\|_2 \leq 4 \exp \{(\log 10K)^{15}\} \leq \exp \{(\log N)^{15}\}, \quad (\text{C.7})$$

which matches (3.13), thereby completing the verification of Theorem 3.6.

C.2 Proof of Theorem 6.1

From Theorem 3.2 and Theorem 3.3, it follows that for any $\mathbf{k} \neq \mathbf{k}'$, the off-diagonal entries of ∂T_N satisfy

$$|\partial(T + \varepsilon B)_N(\mathbf{k}, \mathbf{k}')| \leq (\exp \{-|\mathbf{k} - \mathbf{k}'|^s\} + \exp \{-|\mathbf{k} + \mathbf{k}'|^s\}).$$

Following the operator identity in (6.7), we expand $\partial(T + \varepsilon B)_N^{-1}(\mathbf{k}, \mathbf{k}')$ as a double sum as:

$$\partial(T + \varepsilon B)_N^{-1}(\mathbf{k}, \mathbf{k}') = - \sum_{\mathbf{k}_1 \in \Lambda_N} \sum_{\mathbf{k}_2 \in \Lambda_N} (T + \varepsilon B)_N^{-1}(\mathbf{k}, \mathbf{k}_1) (\partial(T + \varepsilon B)_N)(\mathbf{k}_1, \mathbf{k}_2) (T + \varepsilon B)_N^{-1}(\mathbf{k}_2, \mathbf{k}')$$

By applying the triangle inequality, we obtain:

$$\begin{aligned}
& |\partial(T + \varepsilon B)_N^{-1}(\mathbf{k}, \mathbf{k}')| \\
& \leq \sum_{\mathbf{k}_1 \in \Lambda_N} \sum_{\mathbf{k}_2 \in \Lambda_N} |(T + \varepsilon B)_N^{-1}(\mathbf{k}, \mathbf{k}_1)| \cdot |\partial(T + \varepsilon B)_N(\mathbf{k}_1, \mathbf{k}_2)| \cdot |(T + \varepsilon B)_N^{-1}(\mathbf{k}_2, \mathbf{k}')| \\
& \leq \frac{4N^2(2N+1)^{2n}}{\varepsilon_N^2} \left(\exp \left\{ -\frac{(|\mathbf{k} - \mathbf{k}'| - 2N^{\frac{1}{2}})^s}{2} \right\} + \exp \left\{ -\frac{(|\mathbf{k} + \mathbf{k}'| - 2N^{\frac{1}{2}})^s}{2} \right\} \right),
\end{aligned}$$

where the last inequality follows Theorem B.1. Given that the spatial separation satisfies $|\mathbf{k} \pm \mathbf{k}'| \geq N^{\frac{3}{4}}$, the off-diagonal entries of ∂T_N^{-1} satisfies (6.9). The proof thus is complete.